

Projective studies of spin nematics in a quantum frustrated ferromagnet

Ryuichi Shindou,^{1,2} Seiji Yunoki,^{3,4,5} and Tsutomu Momoi¹

¹Condensed Matter Theory Laboratory, RIKEN, 2-1 Hirosawa, Wako, Saitama 351-0198, Japan

²Physics Department, Tokyo Institute of Technology,
2-12-1 Ookayama, Meguro-ku, Tokyo 152-8551, Japan

³Computational Condensed Matter Laboratory, RIKEN ASI, 2-1 Hirosawa, Wako, Saitama 351-0198, Japan

⁴Computational Materials Science Research Team, RIKEN AICS, Kobe, Hyogo 650-0047, Japan

⁵CREST, Japan Science and Technology Agency (JST), Kawaguchi, Saitama 332-0012, Japan
(Dated: November 7, 2018)

We study the ground state properties of the spin- $\frac{1}{2}$ frustrated ferromagnetic J_1 - J_2 Heisenberg model on the square lattice, employing projected BCS wavefunctions with spin-triplet pairings of the spinon fields as trial wavefunctions. Based on the variational Monte Carlo analysis, we argue that, in the competing coupling regime, a certain type of the projected BCS wavefunction, dubbed the projected Z_2 planar state, achieves the best optimal energy among the other competing states such as the ferromagnetic state and collinear antiferromagnetic state. Like in quantum spin liquids, the projected Z_2 planar state preserves the translational symmetry of the square lattice. However, it is also accompanied by a d -wave ordering of the quadrupole moments, breaking the spin rotational symmetry. The state thus describes a quantum spin analogue of the nematic liquid crystals. The calculated static correlation functions also reveal that the projected Z_2 planar state has a strong collinear antiferromagnetic fluctuation.

PACS numbers:

I. INTRODUCTION

Deciphering unidentified states of quantum zero-point motion – quantum vacuum – is one of the central research field in condensed matter physics.¹ In the realm of quantum magnetism, investigations of *spin-rotational symmetric* quantum spin liquid (QSL) – a quantum magnet which remains totally disordered all the way down to the zero temperature – belong to this research category. Indeed, after seminal proposal of spin-singlet resonating valence bond (RVB) wavefunctions by Anderson and his co-workers,² tremendous research efforts are devoted to establishing a true realization of QSL or RVB-type ground state in spatial dimension greater than one.³ Among others, ‘frustrated’ Mott insulating magnets are regarded as promising candidate materials for this investigation,⁴ where competing magnetic interactions between localized spins often make it hard for a system to fall into a simple classical spin ordering.

This work reports a variational study of spin- $\frac{1}{2}$ quantum frustrated *ferromagnetic* model. One motivation of this research is a couple of experimental works on two-dimensional films of solid ^3He ,^{5,6} where the interactions between $S = \frac{1}{2}$ nuclear spins of ^3He atoms are highly frustrated but predominantly ferromagnetic.⁷ The specific heat measurement⁵ and magnetic susceptibility⁶ at the ultra-low temperature regime conclude that the ground state of this frustrated quantum spin system is a QSL-like state with either a gapless spin excitation or an extremely small spin gap. These experiments suggest a possibility of an exotic quantum phase in quantum frustrated *ferromagnets*.

The other incentive of this work stems from recent theoretical studies of frustrated magnets with ferromag-

netic nearest-neighbor interactions on the square lattice and triangular lattice that report possible realization of spin *nematic* phases.^{8–13} Among frustrated ferromagnets, the spin- $\frac{1}{2}$ square lattice J_1 - J_2 model with ferromagnetic J_1 is a prototype minimal model and attracting interest recently.^{9–11,14–20} The model Hamiltonian

$$H = J_1 \sum_{\langle j, m \rangle} \mathbf{S}_j \cdot \mathbf{S}_m + J_2 \sum_{\langle\langle j, m \rangle\rangle} \mathbf{S}_j \cdot \mathbf{S}_m \quad (1)$$

consists of nearest-neighbor ferromagnetic exchange J_1 (< 0) and competing next-nearest-neighbor antiferromagnetic exchange J_2 (> 0). When the antiferromagnetic coupling is much stronger than that of the ferromagnetic coupling ($|J_1| \ll 2J_2$), the ground state exhibits a collinear antiferromagnetic order, $\langle \mathbf{S}_j \rangle = (-1)^{j_x} \mathbf{m}$ or $(-1)^{j_y} \mathbf{m}$ with $\mathbf{j} = (j_x, j_y)$.²¹ While the ground state in the opposite limit ($|J_1| \gg 2J_2$) is the fully polarized ferromagnetic state. The preceding exact diagonalization studies^{9–11} suggest the existence of the spin nematic phase between these two magnetic ordered phases.

Motivated by these studies, the present authors recently formulated a fermionic mean-field theory for quantum frustrated ferromagnets,¹⁸ where they proposed to describe the quantum spin nematic phase as a *spin-triplet variant* of spin-rotational symmetric quantum spin liquids. The state suggested by this mean-field theory is a ‘mixed’ resonating valence bond (RVB) wavefunction, where all the half-spins in any lattice points belong to either the singlet valence bonds on antiferromagnetic links or the spin-triplet valence bonds introduced on ferromagnetic links. The wavefunction is given by a superposition of different partitioning of spins into either singlet or triplet bonds, such that the wavefunction, on the whole, has no preference for any specific valence bond configu-

ration.

Unlike Néel-ordered states or dimer states, this mixed RVB state preserves the lattice-translational symmetry of the square lattice, indicating its ‘quantum spin liquid’ like character. In contrast to the spin-singlet RVB state, however, the spin-1 moment in the triplet valence bond breaks spin-rotational symmetry, quantum-mechanically rotating within a specific plane. Thus, unlike *spin-rotational symmetric* quantum spin liquids, this mixed RVB state is accompanied by the breakdown of global spin-rotational symmetry. In fact, this spontaneous symmetry breaking manifests itself as the ordering of the quadrupole moment,^{8,9,18,22}

$$K_{j,m}^{\mu\nu} \equiv \frac{1}{2}(S_{j,\mu}S_{m,\nu} + S_{j,\nu}S_{m,\mu}) - \frac{\delta_{\mu\nu}}{3}\langle \mathbf{S}_j \cdot \mathbf{S}_m \rangle, \quad (2)$$

instead of the ordering of the spin dipole moment, i.e., $\langle \mathbf{S}_j \rangle = \mathbf{0}$. In Eq. (2), \mathbf{j} and \mathbf{m} denote two adjacent lattice sites connected by a ferromagnetic link, and μ and ν are the spin indices. Having both quantum spin liquid character and also symmetry breaking phase character, this mixed RVB state is regarded as the *quantum spin* analogue of ‘liquid-crystal’ like state of matter.^{8,9,18,22,23}

To investigate the nature of this unconventional quantum spin state, we study, in this paper, the spin- $\frac{1}{2}$ square lattice J_1 - J_2 Heisenberg model, using the variational Monte Carlo method. Our method is based on the fermionic representation of spin- $\frac{1}{2}$ operators $S_{j,\mu} = \frac{1}{2}f_{j,\alpha}^\dagger[\sigma_\mu]_{\alpha\beta}f_{j,\beta}$ ($\mu = 1, 2, 3$),^{1,24,25} where $f_{j,\alpha}^\dagger$ denotes the fermion creation operator at the site \mathbf{j} with spin α and σ_μ the Pauli matrices. The representation becomes exact, when one and only one fermion is located at every site, i.e., $f_{j,\alpha}^\dagger f_{j,\alpha} = 1$. At the mean-field level, this local constraint on fermions’ number is replaced by their coupling with the chemical potential, so that the only the global constraint is taken into account.

In this fermionic representation, the exchange interaction between two localized spins is written as a four-point interaction, which the mean-field theory decomposes into the pairing fields between two adjacent fermions. The antiferromagnetic exchange interaction is decoupled in terms of the spin-singlet pairing fields as^{1,24-26}

$$\begin{aligned} \mathbf{S}_i \cdot \mathbf{S}_j &\simeq \frac{1}{4}(|\chi_{ij}|^2 + |\eta_{ij}|^2) + \text{const} \\ &+ \frac{1}{4} \left(-\chi_{ji} f_{i,\alpha}^\dagger f_{j,\alpha} - \eta_{ji} f_{i,\alpha}^\dagger [i\sigma_2]_{\alpha\beta} f_{j,\beta}^\dagger + \text{h.c.} \right) \end{aligned} \quad (3)$$

where χ_{ij} denotes the particle-hole (excitonic) pairing field,

$$\chi_{ij} = \langle f_{i,\alpha}^\dagger f_{j,\alpha} \rangle, \quad (4)$$

and η_{ij} is the particle-particle (Cooper) pairing field,

$$\eta_{ij} = \langle f_{i,\alpha} [-i\sigma_2]_{\alpha\beta} f_{j,\beta} \rangle. \quad (5)$$

On the other hand, the competing ferromagnetic exchange interaction should be decoupled into the spin-

triplet channel in its own right,¹⁸

$$\begin{aligned} -\mathbf{S}_i \cdot \mathbf{S}_j &\simeq \frac{1}{4}(|\mathbf{E}_{ij}|^2 + |\mathbf{D}_{ij}|^2) + \text{const.} \\ &+ \frac{1}{4} \sum_{\mu=1}^3 \left(-E_{j\mathbf{i},\mu} f_{i,\alpha}^\dagger [\sigma_\mu]_{\alpha\beta} f_{j,\beta} + \text{h.c.} \right) \\ &+ \frac{1}{4} \sum_{\mu=1}^3 \left(-D_{j\mathbf{i},\mu} f_{i,\alpha}^\dagger [-i\sigma_2]_{\alpha\beta} f_{j,\beta}^\dagger + \text{h.c.} \right), \end{aligned} \quad (6)$$

where $\mathbf{D}_{j\mathbf{m}} = (D_{j\mathbf{m},1}, D_{j\mathbf{m},2}, D_{j\mathbf{m},3})$ denotes the so-called d -vector of the spin-triplet Cooper pairing field,^{29,30}

$$D_{ij,\mu} = \langle f_{i,\alpha} [i\sigma_2]_{\alpha\beta} f_{j,\beta} \rangle, \quad (7)$$

and $\mathbf{E}_{j\mathbf{m}} = (E_{j\mathbf{m},1}, E_{j\mathbf{m},2}, E_{j\mathbf{m},3})$ is the excitonic counterpart of the d -vector,

$$E_{ij,\mu} = \langle f_{i,\alpha}^\dagger [\sigma_\mu]_{\alpha\beta} f_{j,\beta} \rangle. \quad (8)$$

Physically speaking, this decoupling is because the ferromagnetic exchange interaction between two spin halves^{18,27} usually prefers the formation of their spin-triplet valence bond, $|S=1, S_\mu=0\rangle$ ($\mu = 1, 2, 3$), instead of the singlet valence bond. Indeed, the d -vector associated with the triplet pairing specifies the direction along which the spin triplet state has the zero magnetization, i.e. $|S=1, (\mathbf{e}_d \cdot \mathbf{S})=0\rangle$ with $\mathbf{e}_d = \mathbf{D}_{j\mathbf{m}}/|\mathbf{D}_{j\mathbf{m}}|$. One can easily see at the mean-field level that the triplet pairing fields in Eqs. (7) and (8) induce the following quadrupole moment,¹⁸

$$\begin{aligned} \langle K_{i,j}^{\mu\nu} \rangle &= -\frac{1}{2} (E_{ij,\mu} E_{ij,\nu}^* - \frac{1}{3} \delta_{\mu\nu} |\mathbf{E}_{ij}|^2) \\ &- \frac{1}{2} (D_{ij,\mu} D_{ij,\nu}^* - \frac{1}{3} \delta_{\mu\nu} |\mathbf{D}_{ij}|^2) + \text{h.c.} \end{aligned}$$

The previous fermionic mean-field analysis shows that the present square-lattice model, Eq. (1), has five different spin-triplet pairing states as its saddle point solutions:²⁸ (i) Z_2 planar state, (ii) Z_2 polar state, (iii) $SU(2)$ chiral p -wave state and (iv) ‘flat-band’ state, where the first state is accompanied by a ‘coplanar’ or ‘d-wave’ configuration of the quadrupole moments while the second and third ones support ‘collinear’ configurations of the quadrupole moments. Among them, Z_2 planar phase and $SU(2)$ chiral p -wave phase appear, having the lowest energy, in the finite range of competing coupling regime between the ferromagnetic phase and π -flux phase in the mean-field phase diagram.

In this paper, we investigate the nature and energetics of the projected BCS wavefunctions constructed from these mean-field pairing states. As the local constraint of the fermion density is not strictly observed in the mean-field theory, the BCS wavefunctions generally range over the ‘extended’ Hilbert space, which allows double occupancy or vacancy on a single site. To obtain a proper trial many-body wavefunction for the spin model, we first

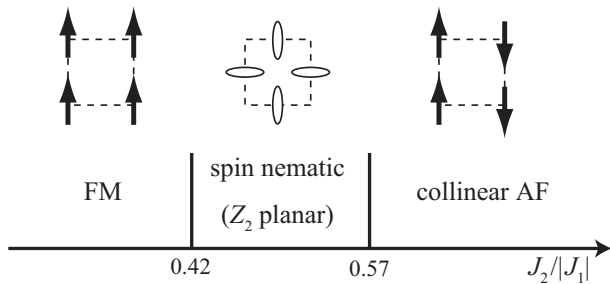


FIG. 1: Phase diagram of the spin-1/2 square lattice J_1 - J_2 model with ferromagnetic (FM) J_1 and antiferromagnetic (AF) J_2 , obtained from variational Monte Carlo simulations.

project these BCS wavefunctions onto the physical spin Hilbert space, imposing the single-fermion condition on every site. By minimizing energies of these *projected* BCS wavefunctions in a variational way, we obtain their optimal energies. Comparing these energies with those of the ferromagnetic state and the collinear antiferromagnetic state, we argue that *only* a projected Z_2 planar state becomes most energetically favorable among the other competing states in a finite range of the intermediate coupling regime, $0.42|J_1| \lesssim J_2 \lesssim 0.57|J_1|$. Our results are summarized in Fig. 1.

Based on this observation, we further study the character of the projected Z_2 planar state. Specifically, we clarify the irreducible representations of this many-body wavefunction under the point group symmetries of the square lattice, and argue that this state is actually accompanied by a ‘ d -wave’ ordering of the quadrupole moments. All irreducible representations and the d -wave character are totally consistent with the nature of the spin nematic phase suggested by the previous exact diagonalization study.⁹ This agreement in combination with the energetics suggests that the projected Z_2 planar state is indeed realized in the intermediate coupling regime of the square lattice J_1 - J_2 model. To give a direct physical characterization to this quantum spin nematic phase, we further calculate the static correlation functions in this projected BCS wavefunction in a large system size (100, 144, and 324 sites). By that, we found that the wavefunction exhibits strong antiferromagnetic fluctuation with the wave vectors $\mathbf{k} = (\pi, 0)$ and $(0, \pi)$ associated with the proximate collinear antiferromagnetic phase, though the finite size scaling suggests that, the state does not possess any staggered sublattice magnetization in the thermodynamic limit.

The remaining sections of this paper are organized as follows: In Sec. II, we briefly review spin-triplet pairing states obtained by the previous fermionic mean-field analysis. We also extend these mean-field solutions into the case under finite external Zeeman field. By this extension, the projected ‘flat-band’ state turns out to be the fully polarized ferromagnetic state. We also find that all the d -vectors in the spin-triplet pairing states are lying within a plane perpendicular to the applied

field. This feature guarantees the ‘spin-nematic’ character of the projected BCS wavefunctions constructed from these pairing states. In Sec. III, we give a general expression for the projected BCS wavefunctions having both spin-triplet and spin-singlet pairings. Based on this expression, we have optimized numerically the energies of (i) projected Z_2 planar state, (ii) projected Z_2 polar state, and (iii) projected $SU(2)$ chiral p -wave state. In Sec. IV, after briefly explaining the method of optimization and Monte Carlo simulations, we compare their optimized energies with other competing states such as the collinear antiferromagnetic state and the fully polarized ferromagnetic state. Sections V and VI contain discussions about the nature of the projected BCS wavefunctions. In Sec. V, we argue that all the projected BCS wavefunctions studied in this paper have a spin-nematic property, i.e., ordering of the quadrupole moments *without* any ordering of spins. We show in particular that the projected Z_2 planar state is accompanied by a d -wave spatial configuration of ordered quadrupole moments. In Sec. VI, we discuss the behavior of the static correlation functions of spins and quadrupole moments calculated in this projected Z_2 planar state. Section VII is devoted to the summary and discussion.

II. MEAN-FIELD ANSATZ UNDER THE FIELD

The J_1 - J_2 frustrated ferromagnetic square lattice model has four types of spin-triplet pairing states as the saddle point solutions of the $SU(2)$ fermionic mean-field theory: (i) Z_2 planar state, (ii) Z_2 polar state, (iii) $SU(2)$ chiral p -wave state and (iv) ‘flat-band’ state, all of which possess the same translational symmetry as the square lattice. We describe in this section how these triplet pairing states are deformed under external Zeeman field. We will see that all the d -vectors in the states (i), (ii) and (iii) are restricted within a plane perpendicular to the applied magnetic field. Because of this arrangement, the mean-field Hamiltonian for these three states are invariant under the spin π -rotation around the field, when combined with the staggered gauge transformation $f_{\mathbf{j},\alpha} \rightarrow (-1)^{j_x+j_y} f_{\mathbf{j},\alpha}$. This symmetry property actually gives the spin-nematic character to the corresponding projected BCS wavefunctions (see Sec. V).

A. Z_2 planar state

In the Z_2 planar state in the absence of magnetic field, the nearest-neighbor ferromagnetic bonds support a coplanar configurations of the d -vector, e.g.,

$$D_{\mathbf{i}\mathbf{j},\mu} = \begin{cases} D\delta_{\mu,1} & (\mathbf{i} = \mathbf{j} + \mathbf{e}_x), \\ D\delta_{\mu,2} & (\mathbf{i} = \mathbf{j} + \mathbf{e}_y), \end{cases} \quad (9a)$$

$$E_{\mathbf{i}\mathbf{j},\mu} = 0 \quad (9b)$$

with $\mathbf{e}_x = (1, 0)$ and $\mathbf{e}_y = (0, 1)$, while the next-nearest neighbor antiferromagnetic bonds support the

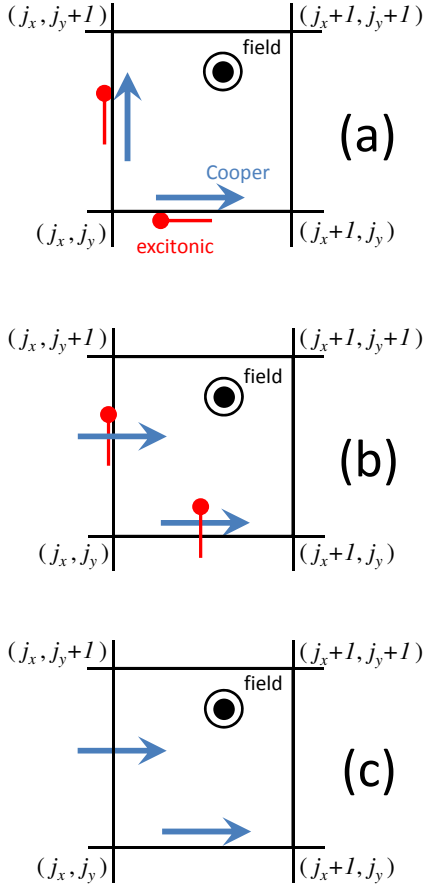


FIG. 2: (Color online) A schematic picture of the spatial configuration of d -vectors in (a) Z_2 planar state, (b) Z_2 polar state and (c) $SU(2)$ chiral p -wave state on the square lattice under the field. The d -vectors in the Cooper channel are drawn by (blue) arrows and those in the excitonic channel are given by (red) round head arrows, both of which are on the nearest-neighbor ferromagnetic bonds. Since all these three states preserve the translational symmetry of the square lattice, we show their configurations in the unit cell. All the d -vectors are lying within the plane perpendicular to the applied field. These three states are invariant under the spin π -rotation around the field, combined with staggered gauge transformation, which guarantees the spin-nematic character of the corresponding projected BCS wavefunctions (see Sec. V).

‘staggered-flux’ configurations of the spin-singlet pairings,³¹

$$\eta_{ij} = \pm\eta, \quad \chi_{ij} = \chi, \quad (10)$$

when $\mathbf{i} = \mathbf{j} + \mathbf{e}_x \pm \mathbf{e}_y$. The corresponding Bogoliubov de-Gennes (BdG) mean-field Hamiltonian has the form

$$\begin{aligned} \mathcal{H}_{\text{planar}} = & \sum_{\mathbf{j}} \left\{ \frac{|J_1|}{4} D \left(-f_{\mathbf{j},\alpha}^\dagger [\sigma_3]_{\alpha\beta} f_{\mathbf{j}+\mathbf{e}_x,\beta}^\dagger + i f_{\mathbf{j},\alpha}^\dagger f_{\mathbf{j}+\mathbf{e}_y,\alpha}^\dagger \right) \right. \\ & - \frac{J_2}{4} \sum_{\sigma=\pm} \left(\chi f_{\mathbf{j},\alpha}^\dagger f_{\mathbf{j}+\mathbf{e}_x+\sigma\mathbf{e}_y,\alpha} + i\sigma\eta f_{\mathbf{j},\alpha}^\dagger [\sigma_2]_{\alpha\beta} f_{\mathbf{j}+\mathbf{e}_x+\sigma\mathbf{e}_y,\beta}^\dagger \right) \\ & \left. + \text{h.c.} \right\}. \quad (11) \end{aligned}$$

This Z_2 planar state is energetically degenerate under spin $SU(2)$ rotation.

In the presence of magnetic field, spin z -component couples to both magnetic field and mean fields from the surrounding spins. This effect can be captured by adding the term $-h_{\text{eff}} \sum_{\mathbf{j}} S_{\mathbf{j},z}$ to the mean-field Hamiltonian. A direct energy optimization suggests that, under the external Zeeman field, the coplanar plane of the d -vectors is restricted within a plane perpendicular to the field. Moreover, the magnetic field gives rise to the excitonic triplet pairing, whose director vectors are also perpendicular to the field, replacing Eq. (9b) with

$$E_{i\mathbf{j},\mu} = \begin{cases} -iE\delta_{\mu,1} & (\mathbf{i} = \mathbf{j} + \mathbf{e}_x), \\ iE\delta_{\mu,2} & (\mathbf{i} = \mathbf{j} + \mathbf{e}_y). \end{cases} \quad (12)$$

The mean-field Hamiltonian has the following form under the field

$$\begin{aligned} \mathcal{H}'_{\text{planar}} = & \mathcal{H}_{\text{planar}} + \sum_{\mathbf{j}} \left\{ \left[i \frac{|J_1|}{4} E \left(f_{\mathbf{j},\alpha}^\dagger [\sigma_1]_{\alpha\beta} f_{\mathbf{j}+\mathbf{e}_x,\beta} \right) \right. \right. \\ & \left. \left. - f_{\mathbf{j},\alpha}^\dagger [\sigma_2]_{\alpha\beta} f_{\mathbf{j}+\mathbf{e}_y,\beta} \right) + \text{h.c.} \right] - \frac{1}{2} h_{\text{eff}} f_{\mathbf{j},\alpha}^\dagger [\sigma_3]_{\alpha\beta} f_{\mathbf{j},\beta} \right\}. \end{aligned}$$

The state preserves the translational symmetry of the square lattice, so that the mean-field Hamiltonian is Fourier-transformed as

$$\begin{aligned} \mathcal{H}'_{\text{planar}} = & \sum_{\mathbf{k}; k_y > 0} \mathbf{f}_{\mathbf{k}} \left\{ -\frac{|J_1|}{2} D (s_x \gamma_3 - s_y \gamma_5) \right. \\ & + \frac{|J_1|}{2} E (s_x \gamma_{23} + s_y \gamma_{25}) - J_2 \chi c_x c_y \gamma_4 \\ & \left. - J_2 \eta s_x s_y \gamma_2 + \frac{1}{2} h_{\text{eff}} \gamma_{35} \right\} \mathbf{f}_{\mathbf{k}}, \quad (13) \end{aligned}$$

where $\mathbf{k} = (k_x, k_y)$, $\mathbf{f}_{\mathbf{k}} \equiv (f_{\mathbf{k},\uparrow}^\dagger, f_{\mathbf{k},\downarrow}^\dagger, f_{-\mathbf{k},\uparrow}, f_{-\mathbf{k},\downarrow})$, $f_{\mathbf{k},\alpha} \equiv \frac{1}{\sqrt{N}} \sum_{\mathbf{j}} e^{i\mathbf{k}\cdot\mathbf{j}} f_{\mathbf{j},\alpha}$, $s_a \equiv \sin k_a$, and $c_a \equiv \cos k_a$ with $a = x, y$. The 4×4 γ -matrices are defined as $\gamma_1 = \sigma_2 \otimes \sigma_1$, $\gamma_2 = \sigma_2 \otimes \sigma_2$, $\gamma_3 = \sigma_2 \otimes \sigma_3$, $\gamma_4 = \sigma_3 \otimes \sigma_0$, $\gamma_5 = \sigma_1 \otimes \sigma_0$, and $\gamma_{jm} = -i\gamma_j \gamma_m$, where the 2×2 Pauli matrices in front of the \otimes -mark is for the particle-hole space, while the others are for the spin space, e.g.

$$\gamma_1 = \begin{pmatrix} 0 & -i\sigma_1 \\ i\sigma_1 & 0 \end{pmatrix}.$$

B. Z_2 polar state

The Z_2 polar state at zero field takes a collinear configuration of the d -vectors on ferromagnetic bonds, e.g.,

$$D_{ij,\mu} = D\delta_{\mu,1}, \quad (14a)$$

$$E_{ij,\mu} = 0 \quad (14b)$$

for $\mathbf{i} = \mathbf{j} + \mathbf{e}_a$ ($a = x, y$), while it supports the same staggered-flux configuration of the singlet pairings as in Eq. (10).

In the presence of magnetic field, the external Zeeman field restricts the d -vectors within its transverse directions the same as in Eq. (14a) and brings about the excitonic spin-triplet pairings, replacing Eq. (14b) with

$$E_{ij,\mu} = iE\delta_{\mu,2} \quad (15)$$

for $\mathbf{i} = \mathbf{j} + \mathbf{e}_a$ ($a = x, y$). The d -vectors of the induced excitonic spin-triplet pairings are perpendicular to both the external field and the d -vectors of the Cooper channel. The mean-field Hamiltonian for the Z_2 polar state has the following form under the field,

$$\begin{aligned} \mathcal{H}_{\text{polar}} = & \sum_{\mathbf{j}} \left\{ \left[\alpha_1 f_{\mathbf{j},\uparrow}^\dagger f_{\mathbf{j},\downarrow}^\dagger \right. \right. \\ & - \frac{|J_1|}{4} \sum_{a=x,y} \left(D f_{\mathbf{j},\alpha}^\dagger [\sigma_3]_{\alpha\beta} f_{\mathbf{j}+\mathbf{e}_a,\beta}^\dagger + iE f_{\mathbf{j},\alpha}^\dagger [\sigma_2]_{\alpha\beta} f_{\mathbf{j}+\mathbf{e}_a,\beta} \right) \\ & - \frac{J_2}{4} \sum_{\sigma=\pm} \left(\chi f_{\mathbf{j},\alpha}^\dagger f_{\mathbf{j}+\mathbf{e}_x+\sigma\mathbf{e}_y,\alpha} + i\sigma\eta f_{\mathbf{j},\alpha}^\dagger [\sigma_2]_{\alpha\beta} f_{\mathbf{j}+\mathbf{e}_x+\sigma\mathbf{e}_y,\beta} \right) \\ & \left. \left. + \text{h.c.} \right] - \frac{1}{2} h_{\text{eff}} f_{\mathbf{j},\alpha}^\dagger [\sigma_3]_{\alpha\beta} f_{\mathbf{j},\beta} \right\}, \quad (16) \end{aligned}$$

where α_1 denotes the uniform temporal gauge field that has a finite value in the Z_2 polar state (see Ref. 18). Or equivalently,

$$\begin{aligned} \mathcal{H}_{\text{polar}} = & \sum_{\mathbf{k}; k_y > 0} \mathbf{f}_{\mathbf{k}}^\dagger \left\{ -\alpha_1 \gamma_2 - \frac{|J_1|}{2} (s_x + s_y) (D\gamma_3 - E\gamma_{25}) \right. \\ & \left. - J_2 \chi c_x c_y \gamma_4 - J_2 \eta s_x s_y \gamma_2 + \frac{1}{2} h_{\text{eff}} \gamma_{35} \right\} \mathbf{f}_{\mathbf{k}}. \quad (17) \end{aligned}$$

C. $SU(2)$ chiral p -wave state

In the $SU(2)$ chiral p -wave state, the d -vectors on the nearest neighbor x -link and that on the y -link are collinear with each other. One of the two acquires an additional phase factor i , compared with the other,

$$D_{ij,\mu} = \begin{cases} D\delta_{\mu,1} & (\mathbf{i} = \mathbf{j} + \mathbf{e}_x), \\ iD\delta_{\mu,1} & (\mathbf{i} = \mathbf{j} + \mathbf{e}_y), \end{cases} \quad (18a)$$

$$E_{ij,\mu} = 0. \quad (18b)$$

Eqs. (18a-b) hold under any magnetic field, provided that the \mathbf{d} -vector is perpendicular to the field.

The antiferromagnetic exchange interaction supports the ‘uniform-RVB’ configuration of the singlet pairings,²⁶

$$\eta_{ij} = 0, \quad \chi_{ij} = \chi \quad (19)$$

for $\mathbf{i} = \mathbf{j} + \mathbf{e}_x \pm \mathbf{e}_y$. The mean-field Hamiltonian for the $SU(2)$ chiral p -wave state takes the following form,

$$\begin{aligned} \mathcal{H}_{\text{chiral } p \text{ wave}} = & \sum_{\mathbf{j}} \left\{ \left[-\frac{|J_1|}{4} D \left(f_{\mathbf{j},\alpha}^\dagger [\sigma_3]_{\alpha\beta} f_{\mathbf{j}+\mathbf{e}_x,\beta}^\dagger \right. \right. \right. \\ & \left. \left. + i f_{\mathbf{j},\alpha}^\dagger [\sigma_3]_{\alpha\beta} f_{\mathbf{j}+\mathbf{e}_y,\beta}^\dagger \right) - \frac{J_2}{4} \chi \sum_{\sigma=\pm} f_{\mathbf{j},\alpha}^\dagger f_{\mathbf{j}+\mathbf{e}_x+\sigma\mathbf{e}_y,\alpha} \right. \\ & \left. \left. + \text{h.c.} \right] - \frac{1}{2} h_{\text{eff}} f_{\mathbf{j},\alpha}^\dagger [\sigma_3]_{\alpha\beta} f_{\mathbf{j},\beta} \right\}, \quad (20) \end{aligned}$$

or equivalently,

$$\begin{aligned} \mathcal{H}_{\text{chiral } p \text{ wave}} = & \sum_{\mathbf{k}; k_y > 0} \mathbf{f}_{\mathbf{k}}^\dagger \left\{ -\frac{|J_1|}{2} D (s_x \gamma_3 + s_y \gamma_{34}) \right. \\ & \left. - J_2 \chi c_x c_y \gamma_4 + \frac{1}{2} h_{\text{eff}} \gamma_{35} \right\} \mathbf{f}_{\mathbf{k}}. \quad (21) \end{aligned}$$

D. Fully polarized state out of ‘flat-band’ states

The ‘flat-band’ states have only spin-triplet pairings on the ferromagnetic bonds, while no spin-singlet pairing on the antiferromagnetic bonds. According to our previous work,¹⁸ this state achieves the best mean-field energy among others in the strongly ferromagnetic regime ($|J_1| \gg J_2$). In the absence of the external field, the triplet pairings in the ‘flat-band’ state are most generally characterized by a $U(1)$ phase, θ , three orthogonal unit vectors $\{\mathbf{n}_1, \mathbf{n}_2, \mathbf{n}_3\}$ in the spin space, and two orthogonal unit vectors $\{\mathbf{m}_1, \mathbf{m}_2\}$ in the gauge space as follows

$$D_{ij} = \begin{cases} \cos \theta \mathbf{n}_1 (m_{1,3} + i m_{1,2}) & (\mathbf{i} = \mathbf{j} + \mathbf{e}_x), \\ \sin \theta \mathbf{n}_1 (m_{2,3} + i m_{2,2}) & (\mathbf{i} = \mathbf{j} + \mathbf{e}_y), \end{cases} \quad (22a)$$

$$E_{ij} = \begin{cases} \cos \theta (\mathbf{n}_2 + i \mathbf{n}_1 m_{1,1}) & (\mathbf{i} = \mathbf{j} + \mathbf{e}_x), \\ \sin \theta (\mathbf{n}_3 + i \mathbf{n}_1 m_{2,1}) & (\mathbf{i} = \mathbf{j} + \mathbf{e}_y), \end{cases} \quad (22b)$$

where

$$\mathbf{n}_1 \cdot \mathbf{n}_2 = \mathbf{n}_2 \cdot \mathbf{n}_3 = \mathbf{n}_3 \cdot \mathbf{n}_1 = 0, \quad (23)$$

$$\mathbf{m}_1 \cdot \mathbf{m}_2 = 0. \quad (24)$$

The energy dispersion of the Bogoliubov particle comprises two bands, which are totally flat in the momentum space and energetically separated by $2|J_1|$ from each other. In the remaining part of this section, we will argue that this state actually reduces to a fully polarized ferromagnetic state, once an infinitesimally small Zeeman field is applied.

Under the Zeeman field, it is energetically favorable that all the d -vectors are perpendicular to the field. To

make this compatible with the orthogonality condition Eq. (23), the $U(1)$ phase θ is going to be locked in $\theta = \frac{\pi}{2}l$ with $l \in \mathbb{Z}$. Namely, when $\theta = \pm \frac{\pi}{2}$, only \mathbf{n}_3 and \mathbf{n}_1 are required to be perpendicular to the field, while, in the case of $\theta = 0$ or π , only \mathbf{n}_1 and \mathbf{n}_2 are perpendicular to the field. Thereby, this locking reduces the ‘flat-band’ state into a decoupled one-dimensional fermion states running along either x -link or y -link. For example, when $\theta = 0$, one of the flat-band states under an infinitesimally small field can be described with $\mathbf{n}_1 = (1, 0, 0)$, $\mathbf{n}_2 = (0, 1, 0)$, and $\mathbf{m}_1 = (1, 0, 0)$. The corresponding BdG Hamiltonian is given as

$$\mathcal{H}_{\text{flat}} = \sum_j \left\{ \left[-\frac{|J_1|}{4} \left(i f_{j,\alpha}^\dagger [\sigma_1]_{\alpha\beta} f_{j+e_x,\beta} + f_{j,\alpha}^\dagger [\sigma_2]_{\alpha\beta} f_{j+e_x,\beta} \right) + \text{h.c.} \right] - \frac{1}{2} h_{\text{eff}} f_{j,\alpha}^\dagger [\sigma_3]_{\alpha\beta} f_{j,\beta} \right\}. \quad (25)$$

Or equivalently,

$$\mathcal{H}_{\text{flat}} = \sum_{j_y=1}^{L_y} \sum_{-\pi < k_x < \pi} \mathbf{f}_{k_x, j_y}^\dagger \left\{ -\frac{|J_1|}{2} (c_x \gamma_{31} + s_x \gamma_{23}) + \frac{1}{2} h_{\text{eff}} \gamma_{35} \right\} \mathbf{f}_{k_x, j_y}, \quad (26)$$

where $\mathbf{f}_{k_x, j_y}^\dagger \equiv (f_{k_x, j_y, \uparrow}^\dagger, f_{k_x, j_y, \downarrow}^\dagger, f_{-k_x, j_y, \uparrow}, f_{-k_x, j_y, \downarrow})$ and

$f_{k_x, j_y, \alpha} \equiv \frac{1}{\sqrt{L_x}} \sum_{j_x=1}^{L_x} e^{ik_x j_x} f_{j, \alpha}$ with $L_x L_y = N$.

When projected into the spin Hilbert space, the ground-state wavefunction of Eq. (26) reduces to a fully polarized ferromagnetic state. To see this, note that it is given by a composite of decoupled one-dimensional fermionic states running along the x -link; $|\Psi_{\text{flat}}\rangle = \prod_{j_y=1}^{L_y} |\Psi_{j_y}\rangle$. For every $j_y = 1, \dots, L_y$, $|\Psi_{j_y}\rangle$ is given by

$$|\Psi_{j_y}\rangle = \prod_{-\pi < k_x < \pi} \left(-\cos \frac{\phi}{2} e^{i\frac{\pi}{4} + i\frac{k_x}{2}} f_{k_x, \uparrow}^\dagger + \sin \frac{\phi}{2} e^{-i\frac{\pi}{4} - i\frac{k_x}{2}} f_{k_x, \downarrow}^\dagger \right) |0\rangle, \quad (27)$$

where $|0\rangle$ denotes the vacuum state of the fermions. We have omitted the index ‘ j_y ’, $f_{k_x, j_y, \alpha}^\dagger \rightarrow f_{k_x, \alpha}^\dagger$, since the argument holds for each j_y independently. Note also that the quantization axis of the spin was taken along the field. The angle ϕ is defined as

$$\phi = \tan^{-1} \left[\frac{|J_1|}{h_{\text{eff}}} \right]$$

in the range $-\frac{\pi}{2} \leq \phi \leq \frac{\pi}{2}$.

The inner-product between $|\Psi_{j_y}\rangle$ and an Ising spin configuration $|\{\sigma_{j_x}\}\rangle \equiv \left\{ \prod_{j_x=1}^{L_x} f_{j_x, \sigma_{j_x}}^\dagger \right\} |0\rangle$ is given by a determinant of the $L_x \times L_x$ matrix,

$$\langle \{\sigma_{j_x}\} | \Psi_{j_y} \rangle = \det \begin{bmatrix} a_{\sigma_1} e^{i\frac{\pi\sigma_1}{4}} e^{i\frac{2\pi}{L_x}(-1+\frac{\sigma_1}{2})} & a_{\sigma_2} e^{i\frac{\pi\sigma_2}{4}} e^{i\frac{2\pi}{L_x}(-2+\frac{\sigma_2}{2})} & \dots & a_{\sigma_{L_x}} e^{i\frac{\pi\sigma_{L_x}}{4}} e^{i\frac{2\pi}{L_x}(-L_x+\frac{\sigma_{L_x}}{2})} \\ a_{\sigma_1} e^{i\frac{\pi\sigma_1}{4}} e^{i\frac{4\pi}{L_x}(-1+\frac{\sigma_1}{2})} & a_{\sigma_2} e^{i\frac{\pi\sigma_2}{4}} e^{i\frac{4\pi}{L_x}(-2+\frac{\sigma_2}{2})} & \dots & a_{\sigma_{L_x}} e^{i\frac{\pi\sigma_{L_x}}{4}} e^{i\frac{4\pi}{L_x}(-L_x+\frac{\sigma_{L_x}}{2})} \\ \vdots & \vdots & \ddots & \vdots \\ a_{\sigma_1} e^{i\frac{\pi\sigma_1}{4}} e^{i2\pi(-1+\frac{\sigma_1}{2})} & a_{\sigma_2} e^{i\frac{\pi\sigma_2}{4}} e^{i2\pi(-2+\frac{\sigma_2}{2})} & \dots & a_{\sigma_{L_x}} e^{i\frac{\pi\sigma_{L_x}}{4}} e^{i2\pi(-L_x+\frac{\sigma_{L_x}}{2})} \end{bmatrix}.$$

where $\sigma = \pm 1$ (\uparrow, \downarrow respectively) with $a_\sigma \equiv -\delta_{\sigma,1} \cos \frac{\phi}{2} + \delta_{\sigma,-1} \sin \frac{\phi}{2}$. This determinant becomes non-zero, if and only if all the spins are pointing upward or pointing downward: otherwise, the $L_x \times L_x$ matrix always has two adjacent column-vectors which are parallel to each other in the L_x dimensional space, at a domain wall with $(\sigma_l, \sigma_{l+1}) = (-1, 1)$. Accordingly, we have

$$\langle \{\sigma_{j_x}\} | \Psi_{j_y} \rangle = \left(-\cos \frac{\phi}{2} \right)^{L_x} \prod_{j_x=1}^{L_x} \delta_{\sigma_{j_x}, +1} + \left(\sin \frac{\phi}{2} \right)^{L_x} \prod_{j_x=1}^{L_x} \delta_{\sigma_{j_x}, -1}. \quad (28)$$

Note that $\cos \frac{\phi}{2} > \sin \frac{\phi}{2} \geq 0$ for $h_{\text{eff}} > 0$. This suggests that, when normalized in the thermodynamic limit,

Eq. (27) always reduces to the ferromagnetic state,

$$\lim_{L_x \rightarrow \infty} \frac{1}{\sqrt{\langle \Psi_{j_y} | \Psi_{j_y} \rangle}} |\Psi_{j_y}\rangle = |\uparrow, \uparrow, \dots, \uparrow\rangle \quad (29)$$

for any $j_y = 1, \dots, L_y$.

III. TRIAL MANY-BODY WAVEFUNCTION

As shown in the previous section, the projected ‘flat-band’ state under an infinitesimally small field reduces to the fully polarized ferromagnetic state. As such, we regard that the projected ‘flat-band’ state in the absence of the field is the trivial ferromagnetic state, whose energy is exactly estimated as $-\frac{1}{2}(|J_1| - J_2)$ (per site). Hence we will focus on the character and energetics of the other three spin-triplet RVB states, (i) Z_2 planar state, (ii) Z_2

polar state and (iii) $SU(2)$ chiral p -wave state. To this end, we will construct in this section the *projected* spin-triplet BCS wavefunctions out of their respective mean-field Hamiltonians.

A. Projected spin-triplet BCS wavefunctions

Let us first derive a BCS ‘many-body’ wavefunction for the BdG Hamiltonian which has both spin-triplet and spin-singlet pairings and hopping integrals. Suppose that we have a mean-field Hamiltonian $\mathcal{H} \equiv \sum_{\mathbf{k}; k_y > 0} \mathbf{f}_{\mathbf{k}}^\dagger \mathbf{H}_{\mathbf{k}} \mathbf{f}_{\mathbf{k}}$ and a 4×4 matrix $\mathbf{H}_{\mathbf{k}}$ is diagonalized by a unitary transformation $\mathbf{U}_{\mathbf{k}}$. We typically use Eqs. (13,17,21) for \mathcal{H} . For these Hamiltonians, the eigenvalues always appear in the particle-hole pairwise manner,

$$\mathbf{H}_{\mathbf{k}} \mathbf{U}_{\mathbf{k}} = \mathbf{U}_{\mathbf{k}} \begin{bmatrix} \lambda_{\mathbf{k},1} & & & \\ & \lambda_{\mathbf{k},2} & & \\ & & -\lambda_{\mathbf{k},2} & \\ & & & -\lambda_{\mathbf{k},1} \end{bmatrix}. \quad (30)$$

As such, without loss of generality, we can assume $\lambda_{\mathbf{k},j}$ ($j = 1, 2$) to be positive (semi-)definite. Defining the Bogoliubov particle $\gamma_{\mathbf{k},j}^{(\dagger)}$ ($j = 1, 2$) as

$$\begin{pmatrix} \gamma_{\mathbf{k},1}^\dagger & \gamma_{\mathbf{k},2}^\dagger & \gamma_{-\mathbf{k},2} & \gamma_{-\mathbf{k},1} \end{pmatrix} \equiv \begin{pmatrix} f_{\mathbf{k},\uparrow}^\dagger & f_{\mathbf{k},\downarrow}^\dagger & f_{-\mathbf{k},\uparrow} & f_{-\mathbf{k},\downarrow} \end{pmatrix} \mathbf{U}_{\mathbf{k}}, \quad (31)$$

we obtain

$$\mathcal{H} = \sum_{j=1}^2 \sum_{\mathbf{k}; k_y > 0} \{ \lambda_{\mathbf{k},j} \gamma_{\mathbf{k},j}^\dagger \gamma_{\mathbf{k},j} - \lambda_{\mathbf{k},j} \gamma_{-\mathbf{k},j} \gamma_{-\mathbf{k},j}^\dagger \}. \quad (32)$$

Since $\lambda_{\mathbf{k},j} \geq 0$, the mean-field ground state wavefunction $|\text{g.s.}\rangle$ is a vacuum of the Bogoliubov particles, i.e., $\gamma_{\mathbf{k},j} |\text{g.s.}\rangle = \gamma_{-\mathbf{k},j} |\text{g.s.}\rangle = 0$ for any \mathbf{k} and j , which leads to

$$|\text{g.s.}\rangle \propto \prod_{\mathbf{k}; k_y > 0} \{ \gamma_{\mathbf{k},1} \gamma_{\mathbf{k},2} \gamma_{-\mathbf{k},2} \gamma_{-\mathbf{k},1} \} |0\rangle. \quad (33)$$

Substituting Eq. (31) into Eq. (33), one can easily obtain

$$\begin{aligned} & \prod_{\mathbf{k}; k_y > 0} \{ \gamma_{\mathbf{k},1} \gamma_{\mathbf{k},2} \gamma_{-\mathbf{k},2} \gamma_{-\mathbf{k},1} \} |0\rangle \\ &= c \prod_{\mathbf{k}; k_y > 0} \{ 1 + a_{\mathbf{k}} f_{-\mathbf{k},\uparrow}^\dagger f_{\mathbf{k},\downarrow}^\dagger + b_{\mathbf{k}} f_{-\mathbf{k},\downarrow}^\dagger f_{\mathbf{k},\uparrow}^\dagger \\ &+ a'_{\mathbf{k}} f_{-\mathbf{k},\uparrow}^\dagger f_{\mathbf{k},\uparrow}^\dagger + b'_{\mathbf{k}} f_{-\mathbf{k},\downarrow}^\dagger f_{\mathbf{k},\uparrow}^\dagger + c_{\mathbf{k}} f_{-\mathbf{k},\uparrow}^\dagger f_{-\mathbf{k},\downarrow}^\dagger f_{\mathbf{k},\uparrow}^\dagger f_{\mathbf{k},\downarrow}^\dagger \} |0\rangle \end{aligned} \quad (34)$$

with

$$\begin{aligned} c &= \prod_{k_y > 0} \{ -[\mathbf{U}_{\mathbf{k}}]_{1,3} [\mathbf{U}_{\mathbf{k}}]_{2,4} + [\mathbf{U}_{\mathbf{k}}]_{2,3} [\mathbf{U}_{\mathbf{k}}]_{1,4} \} \\ &\times \{ [\mathbf{U}_{\mathbf{k}}]_{1,1}^* [\mathbf{U}_{\mathbf{k}}]_{2,2}^* - [\mathbf{U}_{\mathbf{k}}]_{1,2}^* [\mathbf{U}_{\mathbf{k}}]_{2,1}^* \} \end{aligned} \quad (35)$$

and

$$\begin{aligned} a_{\mathbf{k}} &= \frac{[\mathbf{U}_{\mathbf{k}}]_{1,1}^* [\mathbf{U}_{\mathbf{k}}]_{3,2}^* - [\mathbf{U}_{\mathbf{k}}]_{1,2}^* [\mathbf{U}_{\mathbf{k}}]_{3,1}^*}{[\mathbf{U}_{\mathbf{k}}]_{1,1}^* [\mathbf{U}_{\mathbf{k}}]_{2,2}^* - [\mathbf{U}_{\mathbf{k}}]_{1,2}^* [\mathbf{U}_{\mathbf{k}}]_{2,1}^*}, \\ b_{\mathbf{k}} &= \frac{[\mathbf{U}_{\mathbf{k}}]_{1,1}^* [\mathbf{U}_{\mathbf{k}}]_{4,2}^* - [\mathbf{U}_{\mathbf{k}}]_{1,2}^* [\mathbf{U}_{\mathbf{k}}]_{4,1}^*}{[\mathbf{U}_{\mathbf{k}}]_{1,1}^* [\mathbf{U}_{\mathbf{k}}]_{2,2}^* - [\mathbf{U}_{\mathbf{k}}]_{1,2}^* [\mathbf{U}_{\mathbf{k}}]_{2,1}^*}, \\ a'_{\mathbf{k}} &= -\frac{[\mathbf{U}_{\mathbf{k}}]_{2,1}^* [\mathbf{U}_{\mathbf{k}}]_{3,2}^* - [\mathbf{U}_{\mathbf{k}}]_{2,2}^* [\mathbf{U}_{\mathbf{k}}]_{3,1}^*}{[\mathbf{U}_{\mathbf{k}}]_{1,1}^* [\mathbf{U}_{\mathbf{k}}]_{2,2}^* - [\mathbf{U}_{\mathbf{k}}]_{1,2}^* [\mathbf{U}_{\mathbf{k}}]_{2,1}^*}, \\ b'_{\mathbf{k}} &= -\frac{[\mathbf{U}_{\mathbf{k}}]_{2,1}^* [\mathbf{U}_{\mathbf{k}}]_{4,2}^* - [\mathbf{U}_{\mathbf{k}}]_{2,2}^* [\mathbf{U}_{\mathbf{k}}]_{4,1}^*}{[\mathbf{U}_{\mathbf{k}}]_{1,1}^* [\mathbf{U}_{\mathbf{k}}]_{2,2}^* - [\mathbf{U}_{\mathbf{k}}]_{1,2}^* [\mathbf{U}_{\mathbf{k}}]_{2,1}^*}, \\ c_{\mathbf{k}} &= -\frac{[\mathbf{U}_{\mathbf{k}}]_{3,1}^* [\mathbf{U}_{\mathbf{k}}]_{4,2}^* - [\mathbf{U}_{\mathbf{k}}]_{3,2}^* [\mathbf{U}_{\mathbf{k}}]_{4,1}^*}{[\mathbf{U}_{\mathbf{k}}]_{1,1}^* [\mathbf{U}_{\mathbf{k}}]_{2,2}^* - [\mathbf{U}_{\mathbf{k}}]_{1,2}^* [\mathbf{U}_{\mathbf{k}}]_{2,1}^*}. \end{aligned} \quad (36)$$

Notice that $c_{\mathbf{k}} = a_{\mathbf{k}} b'_{\mathbf{k}} - a'_{\mathbf{k}} b_{\mathbf{k}}$. This makes it possible to exponentiate the right hand side of Eq. (34) as

$$|\text{g.s.}\rangle \equiv \exp \left[\sum_{\mathbf{k}; k_y > 0} [\mathbf{t}_{\mathbf{k}}]_{\alpha\beta} f_{-\mathbf{k},\alpha}^\dagger f_{\mathbf{k},\beta}^\dagger \right] |0\rangle \quad (37)$$

with

$$\mathbf{t}_{\mathbf{k}} \equiv \begin{bmatrix} a'_{\mathbf{k}} & a_{\mathbf{k}} \\ b'_{\mathbf{k}} & b_{\mathbf{k}} \end{bmatrix}. \quad (38)$$

Equation (37) generally has a finite weight not only on physical (i.e. spin) Hilbert space but also on those fermionic states having either double occupancy on a single site or an empty site. To obtain a variational many-body wavefunction in the physical spin Hilbert space, we need to project out these unphysical fermionic states, imposing ‘single-fermion condition’ on every site;

$$|\Psi_{\alpha}\rangle \equiv \mathcal{P} |\text{g.s.}\rangle, \quad (39)$$

where \mathcal{P} stands for the projection operator onto the physical spin Hilbert space. The projected BCS wavefunction $|\Psi_{\alpha}\rangle$ depends on the pairing and hopping fields encoded in the BdG Hamiltonian, such as D , E , χ , η and h_{eff} . The characteristic of the mean fields is symbolically represented by the subscript α .

Within the spin Hilbert space, the wavefunction is expressed by its inner-product with an Ising spin configuration, $|\{\sigma_j\}\rangle = \{ \prod_j f_{j,\sigma_j}^\dagger \} |0\rangle$. This product generally reduces to a Pfaffian,^{32,35,36}

$$\langle \{\sigma_j\} | \Psi_{\alpha} \rangle = \text{Pf} [\mathbf{X}_{\alpha}(\{\sigma_j\})], \quad (40)$$

where $\mathbf{X}_{\alpha}(\{\sigma_j\})$ denotes the $N \times N$ antisymmetric matrix given by^{35,36}

$$\begin{aligned} [\mathbf{X}_{\alpha}(\{\sigma_j\})]_{j,l} &\equiv [\mathbf{t}(\mathbf{j}, \mathbf{l})]_{\sigma_j, \sigma_l} - [\mathbf{t}(\mathbf{l}, \mathbf{j})]_{\sigma_l, \sigma_j}, \\ [\mathbf{t}(\mathbf{j}, \mathbf{l})]_{\alpha, \beta} &\equiv \frac{1}{N} \sum_{\mathbf{k}; k_y > 0} e^{i\mathbf{k} \cdot (\mathbf{j} - \mathbf{l})} [\mathbf{t}_{\mathbf{k}}]_{\alpha, \beta}. \end{aligned} \quad (41)$$

Note that the boundary condition for the momentum \mathbf{k} remains arbitrary in Eq. (41). To fix this arbitrariness, let

us require that the spin wavefunction given by Eq. (40) is an eigenstate of translations,

$$\langle \{\sigma_{T_a(\mathbf{j})}\} | \Psi_\alpha \rangle = e^{i\theta_a} \langle \{\sigma_{\mathbf{j}}\} | \Psi_\alpha \rangle, \quad (42)$$

where T_a denotes the lattice translational operation by \mathbf{e}_a , i.e., $T_a(\mathbf{j}) = \mathbf{j} + \mathbf{e}_a$ ($a = x, y$). In fact, the preceding exact diagonalization studies³⁷ suggest that the states with non-zero Q vectors are unlikely realized in any intermediate coupling regime of the present J_1 – J_2 model, so that we impose the translational invariance $(e^{i\theta_x}, e^{i\theta_y}) = (1, 1)$ on Eq. (42). To satisfy this requirement, the fermion's momenta in Eq. (41) have only to observe either the anti-periodic boundary condition (APBC), i.e., $k_a = (2n_a - 1)\pi/L_a$ with $n_a = -L_a/2 + 1, \dots, L_a/2$, or the periodic boundary condition (PBC), i.e., $k_a = 2n_a\pi/L_a$. For the two-dimensional models, the trial wavefunctions have four options. When both k_x and k_y satisfy the anti-periodic boundary condition, the total momentum carried by our trial spin wavefunction is indeed at the Γ -point, i.e. $(e^{i\theta_x}, e^{i\theta_y}) = (1, 1)$; to see this, one has only to relate $\mathbf{X}_\alpha(\{\sigma_{T_a(\mathbf{j})}\})$ with $\mathbf{X}_\alpha(\{\sigma_{\mathbf{j}}\})$ in terms of a certain elementary row/column operation O_a ,

$$\mathbf{X}_\alpha(\{\sigma_{T_a(\mathbf{j})}\}) = O_a^T \mathbf{X}_\alpha(\{\sigma_{\mathbf{j}}\}) O_a,$$

where O_a exchanges site indices of $\mathbf{X}_\alpha(\{\sigma_{\mathbf{j}}\})$ according to the lattice translation operator T_a . Similarly, when k_x satisfies the periodic boundary condition while k_y does the anti-periodic boundary condition or vice versa, the momenta carried by the projected BCS wavefunction can be shown to be $(e^{i\theta_x}, e^{i\theta_y}) = ((-1)^{(L_y-1)L_x}, 1)$ or $(e^{i\theta_x}, e^{i\theta_y}) = (1, (-1)^{(L_x-1)L_y})$, respectively. In what follows, we only consider the systems with even length L_x and L_y , to impose the translational invariance of the total wavefunction, i.e., $(e^{i\theta_x}, e^{i\theta_y}) = (1, 1)$.

Notice also that, when both k_x and k_y observe the periodic boundary condition, any of the projected BCS wavefunctions derived from Eqs. (13,17,21) cannot be expressed in terms of a single Pfaffian. This is roughly because, being either d -wave or p -wave, all the pairing fields in the Cooper channel always vanish at the four time-reversal invariant momentums points $(0, 0)$, $(0, \pi)$, $(\pi, 0)$ and (π, π) , where a 4×4 BdG Hamiltonian reduces to a 2×2 Bloch Hamiltonian having no anomalous part. As a result, the state-basis representation of the projected BCS wavefunction becomes relatively cumbersome. In this paper, we study only those projected BCS wavefunctions derived based on the other three boundary conditions. Following the standard literature,^{1,24} we name the projected BCS wavefunction defined with the APBC in the both direction as the ‘wavefunction in the (π, π) -topological sector’ and that with the PBC in one direction and the APBC in the other as the ‘wavefunction in the $(0, \pi)$ or $(\pi, 0)$ -topological sector.’

B. Quantum spin number projection

Our Hamiltonian has the global $SU(2)$ spin rotational symmetry, while the trial wavefunctions constructed from spin-triplet pairing states explicitly break this continuous symmetry by hand. Such a symmetry breaking is supposed to occur only in the thermodynamic limit. The ground-state wavefunction in a finite-size system can be always identified as an eigenstate of the symmetry groups of the Hamiltonian. Accordingly, it is naturally expected that the energy of the trial state will be further improved, when the state being projected onto the eigenspace of an appropriate quantum number associated with the spin-rotational symmetries. Thus, we also consider as our trial state the projections of the spin-triplet BCS wavefunctions with *the quantum spin numbers*.

The spin projection operator which filters out a state with the total spin $S = L$ and the z -component of the total spin $S_z = M$ has a form^{38,39}

$$\mathcal{P}_{S_z=M} \mathcal{P}_{S=L} \equiv \frac{2L+1}{8\pi^2} \int_0^{2\pi} d\alpha \int_0^\pi d\beta \sin\beta \int_0^{2\pi} d\gamma \times P_L(\cos\beta) e^{i\alpha(\hat{S}_z-M)} e^{i\beta\hat{S}_y} e^{i\gamma\hat{S}_z}, \quad (43)$$

where P_L denotes the L -th Legendre polynomial, and $\mathcal{P}_{S=L}$ and $\mathcal{P}_{S_z=M}$ denote the projection operators filtering out a state with the total spin $S = L$ and a state with the z -component of the total spin $S_z = M$, respectively.

Combining this with Eqs. (37)–(41), we obtain the projected BCS wavefunction with the quantum spin number projection as

$$\langle \{\sigma_{\mathbf{j}}\} | \mathcal{P}_{S_z=M} \mathcal{P}_{S=L} | \Psi_\alpha \rangle = \frac{2L+1}{4\pi} \times \int_0^\pi d\beta \sin\beta \int_0^{2\pi} d\gamma P_L(\cos\beta) \text{Pf}[\mathbf{X}_\alpha(\{\sigma_{\mathbf{j}}\}; \beta, \gamma)] \quad (44)$$

under the condition $\frac{1}{2} \sum_{\mathbf{j}} \sigma_{\mathbf{j}} = M$. Here, the $N \times N$ antisymmetric matrix $\mathbf{X}_\alpha(\{\sigma_{\mathbf{j}}\}; \beta, \gamma)$ is defined the same as in Eq. (41) with the 2×2 matrix $\mathbf{t}(\mathbf{j}, \mathbf{l})$ being redefined in a rotated spin frame;

$$[\mathbf{X}_\alpha(\{\sigma_{\mathbf{j}}\}; \beta, \gamma)]_{\mathbf{j}, \mathbf{l}} \equiv [\mathbf{V}_{\beta, \gamma} \mathbf{t}(\mathbf{j}, \mathbf{l}) \mathbf{V}_{\beta, \gamma}^{-1}]_{\sigma_{\mathbf{j}}, \sigma_{\mathbf{l}}} - [\mathbf{V}_{\beta, \gamma} \mathbf{t}(\mathbf{l}, \mathbf{j}) \mathbf{V}_{\beta, \gamma}^{-1}]_{\sigma_{\mathbf{l}}, \sigma_{\mathbf{j}}}, \quad (45)$$

where

$$\mathbf{V}_{\beta, \gamma} \equiv \begin{bmatrix} \cos \frac{\beta}{2} & -\sin \frac{\beta}{2} \\ \sin \frac{\beta}{2} & \cos \frac{\beta}{2} \end{bmatrix} \begin{bmatrix} e^{i\frac{\gamma}{2}} & 0 \\ 0 & e^{-i\frac{\gamma}{2}} \end{bmatrix}.$$

To integrate over β and γ numerically in Eq. (44), we employ the Gauss-Legendre quadrature. When projecting into the singlet space, i.e. $S = 0$, with the system size $N = 6 \times 6 \sim 12 \times 12$, we typically used $10 \sim 16$ mesh points for the integration over β and $10 \sim 20$ mesh points for that of γ .⁴⁰

IV. ENERGY OPTIMIZATION AND ENERGETICS

In this section, we optimize the energies of the projected (i) Z_2 planar state, (ii) Z_2 polar state and (iii) $SU(2)$ chiral p -wave state and compare their minimized energies with those of the ferromagnetic state and the collinear antiferromagnetic state. Specifically, we have numerically calculated the expectation values of the energy for these projected BCS wavefunctions, taking the quantum spin number projection onto the subspace with either $S_z = 0$ or $S = 0$;

$$E_{\alpha}^{S_z=0} = \frac{\langle \Psi_{\alpha} | \mathcal{P}_{S_z=0} H \mathcal{P}_{S_z=0} | \Psi_{\alpha} \rangle}{\langle \Psi_{\alpha} | \mathcal{P}_{S_z=0} | \Psi_{\alpha} \rangle} \quad (46)$$

and

$$E_{\alpha}^{S=0} = \frac{\langle \Psi_{\alpha} | \mathcal{P}_{S=0} H \mathcal{P}_{S=0} | \Psi_{\alpha} \rangle}{\langle \Psi_{\alpha} | \mathcal{P}_{S=0} | \Psi_{\alpha} \rangle}. \quad (47)$$

We have further optimized these energies, tuning the variational parameters α encoded in the original BCS wavefunctions, such as D , E , χ , η and h_{eff} . For this optimization, we have employed the so-called stochastic reconfiguration method.^{33,34}

A. Stochastic reconfiguration method

Here we briefly review the stochastic reconfiguration (SR) method.^{33,34} In this optimization method, a usual steepest descent (SD) method is modified in such a way that information of the ‘quantum distance’ between wavefunctions is included. The quantum distance is chosen to be the square distance between two normalized wavefunctions defined in two different parameter points, say α and $\alpha + \delta\alpha$, in the form

$$\Delta_{\text{SR}}^2 \equiv \left[\langle \overline{\Psi}_{\alpha+\delta\alpha} | - \langle \overline{\Psi}_{\alpha} | \right] \left[| \overline{\Psi}_{\alpha+\delta\alpha} \rangle - | \overline{\Psi}_{\alpha} \rangle \right] \quad (48)$$

with

$$| \overline{\Psi}_{\alpha} \rangle = | \Psi_{\alpha} \rangle \{ \langle \Psi_{\alpha} | \Psi_{\alpha} \rangle \}^{-\frac{1}{2}}.$$

Regarding $|\delta\alpha|$ as a small quantities, we can expand this quantum distance in terms of $\delta\alpha$,

$$\Delta_{\text{SR}}^2 = \sum_{j,m} \delta\alpha_j \delta\alpha_m [\mathbf{S}_{\alpha}]_{j,m} + \mathcal{O}(\delta\alpha^3), \quad (49)$$

where the metric tensor $[\mathbf{S}_{\alpha}]$ is defined in the variational parameter space as

$$[\mathbf{S}_{\alpha}]_{j,m} \equiv \langle \partial_{\alpha_j} \overline{\Psi}_{\alpha} | \partial_{\alpha_m} \overline{\Psi}_{\alpha} \rangle + \text{c.c.} \quad (50)$$

In the standard steepest descent (SD) method, the variational parameters are changed along the gradient of an energy, $\delta\alpha_j = \lambda \partial_{\alpha_j} E_{\alpha}$ with $E_{\alpha} = \langle \overline{\Psi}_{\alpha} | H | \overline{\Psi}_{\alpha} \rangle$ and a

small positive value λ . Meanwhile, the SR method determines the optimal direction, by minimizing the energy *on the contour-(super)sphere of the equal quantum distance*. A variational principle with constraint dictates that the optimal direction thus defined is given by $\delta\alpha_j = \lambda \sum_m [\mathbf{S}_{\alpha}^{-1}]_{j,m} \partial_{\alpha_m} E_{\alpha}$. It is empirically recognized that the modification in terms of the metric tensor $[\mathbf{S}_{\alpha}]$ substantially improves the optimization efficiency, especially when the tensor has a highly non-flat structure in the variational parameter space.^{33,34}

The numerical evaluation of the metric tensor and the gradient vector requires the summation over all the Ising spin configurations in the physical Hilbert space,

$$[\mathbf{S}_{\alpha}]_{m,n} = \frac{1}{2} \sum_{\{\sigma_j\}} (\mathcal{O}_{m,\{\sigma_j\}}^* \mathcal{O}_{n,\{\sigma_j\}} + \text{c.c.}) w_{\{\sigma_j\}} - \sum_{\{\sigma_j\}} \text{Re} \mathcal{O}_{m,\{\sigma_j\}} w_{\{\sigma_j\}} \sum_{\{\sigma_m\}} \text{Re} \mathcal{O}_{n,\{\sigma_m\}} w_{\{\sigma_m\}}, \quad (51)$$

$$\partial_{\alpha_m} E_{\alpha} = \sum_{\{\sigma_j\}} (\mathcal{E}_{\{\sigma_j\}} \mathcal{O}_{m,\{\sigma_j\}} + \text{c.c.}) \omega_{\{\sigma_j\}} - 2 \sum_{\{\sigma_j\}} \text{Re} \mathcal{O}_{m,\{\sigma_j\}} w_{\{\sigma_j\}} \sum_{\{\sigma_m\}} \text{Re} \mathcal{E}_{\{\sigma_m\}} w_{\{\sigma_m\}}, \quad (52)$$

where

$$w_{\{\sigma_j\}} = \frac{|\langle \{\sigma_j\} | \Psi_{\alpha} \rangle|^2}{\langle \Psi_{\alpha} | \Psi_{\alpha} \rangle}, \quad (53)$$

$$\mathcal{O}_{m,\{\sigma_j\}} = \frac{\langle \{\sigma_j\} | \partial_{\alpha_m} \Psi_{\alpha} \rangle}{\langle \{\sigma_j\} | \Psi_{\alpha} \rangle}, \quad (54)$$

$$\mathcal{E}_{\{\sigma_j\}} = \frac{\langle \Psi_{\alpha} | H | \{\sigma_j\} \rangle}{\langle \Psi_{\alpha} | \{\sigma_j\} \rangle}. \quad (55)$$

The SR method replaces this extensive summation by the statistical average where $w_{\{\sigma_j\}}$ is regarded as a probability density of the corresponding statistical ensemble. Specifically, we numerically create a Markov chain in which a binary configuration $\{\sigma_j\}$ is statistically generated with the probability $w_{\{\sigma_j\}}$. In the statistical ensemble thus defined, observables defined in Eqs. (54-55) are numerically evaluated;

$$[\mathbf{S}_{\alpha}]_{m,n} = \frac{1}{2} (\overline{\mathcal{O}_m \mathcal{O}_n^*} + \text{c.c.}) - \frac{1}{4} (\overline{\mathcal{O}_m} + \text{c.c.}) (\overline{\mathcal{O}_n} + \text{c.c.}),$$

$$\partial_{\alpha_m} E_{\alpha} = (\overline{\mathcal{E} \mathcal{O}_m^*} + \text{c.c.}) - \frac{1}{2} (\overline{\mathcal{E}} + \text{c.c.}) (\overline{\mathcal{O}_m} + \text{c.c.}).$$

To obtain the metric tensors and gradient vector, we usually take 1000 ~ 4000 samplings per site. For a set of optimized variational parameters, we evaluate the energy (sec. IVB) and the correlation function (sec. VI), where we typically use 10^5 samplings. As for the projected BCS wavefunction with the quantum spin number projection, one has only to replace $|\Psi_{\alpha}\rangle$ in Eqs. (53)–(55) by $\mathcal{P}_{S_z=M} \mathcal{P}_{S=L} |\Psi_{\alpha}\rangle$. Those who are interested in the actual evaluation of these observables can consult Refs. 36 and 38.

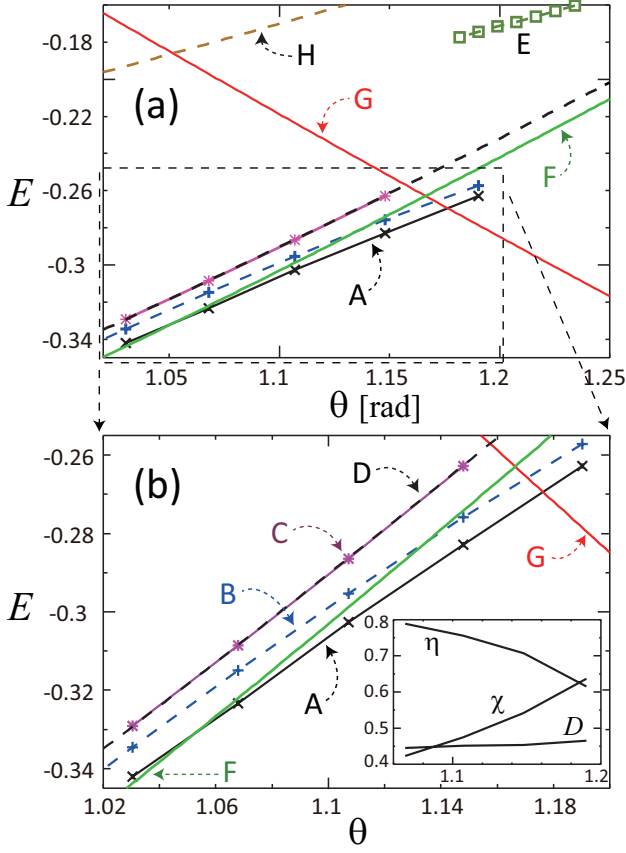


FIG. 3: (Color online) Energy comparison in the square lattice J_1 - J_2 model as a function of θ with $(J_1, J_2) = (-\sin\theta, \cos\theta)$. (a): Optimized energies of the planar states [(A) $\mathcal{P}_{S_z=0}|\Psi_{\text{planar}}\rangle$ and (B) $\mathcal{P}_{S_z=0}|\Psi_{\text{planar}}\rangle$], the polar state [(C) $\mathcal{P}_{S_z=0}|\Psi_{\text{polar}}\rangle$], the π -flux state [(D) $\mathcal{P}_{S_z=0}|\Psi_{\pi\text{-flux}}\rangle$], the p -wave chiral state [(E) $\mathcal{P}_{S_z=0}|\Psi_{\text{chiral}}\rangle$], and the collinear antiferromagnetic state (F). The exact energies of the ferromagnetic state (G) and the isolated dimer state (H) are also shown. The projected state $\mathcal{P}_{S_z=0}|\Psi_{\text{planar}}\rangle$ is calculated in 8×8 spin system and $\mathcal{P}_{S_z=0}|\Psi_{\text{planar}}\rangle$ is in 10×10 spin system. (b): A part of figure (a) is enlarged. (inset): Optimized parameter values of D , χ , and η in $\mathcal{P}_{S_z=0}|\Psi_{\text{planar}}\rangle$ as a function of θ . These values are rescaled, such that $\sqrt{D^2 + \chi^2 + \eta^2} = 1$. The optimal values of the excitonic spin-triplet pairing field E and the effective Zeeman field h_{eff} are negligibly small.

B. Energetics

Figure 3 shows the optimized energies of the projected Z_2 planar states (both $\mathcal{P}_{S_z=0}|\Psi_{\text{planar}}\rangle$ and $\mathcal{P}_{S=0}|\Psi_{\text{planar}}\rangle$), the projected Z_2 polar state $\mathcal{P}_{S_z=0}|\Psi_{\text{polar}}\rangle$, and the projected $SU(2)$ chiral p -wave state $\mathcal{P}_{S_z=0}|\Psi_{\text{chiral}}\rangle$. We also compare these optimized energies with the exact energy of the fully polarized ferromagnetic state $E_{\text{ferro}} = -0.5(|J_1| - J_2)$, and the variationally optimized energies of the collinear antiferromagnetic state⁴² $E_{\text{CAF}} = -0.6682J_2$ and the decoupled double π -flux state⁴¹ $E_{\pi\text{-flux}} = -0.64J_2$. The collinear antiferromagnetic state we considered in this

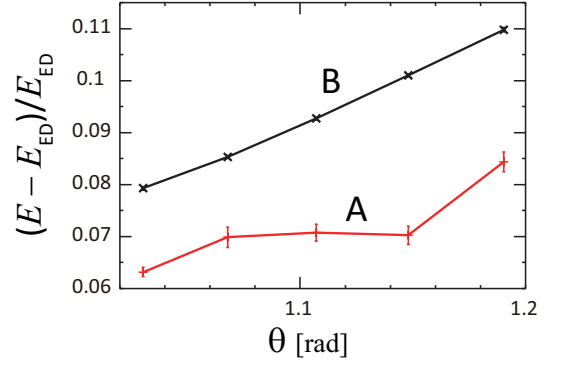


FIG. 4: (Color online) Comparison between the optimized energies of the projected planar states (A) $\mathcal{P}_{S_z=0}|\Psi_{\text{planar}}\rangle$ and (B) $\mathcal{P}_{S_z=0}|\Psi_{\text{planar}}\rangle$, and the ground state energy E_{ED} obtained by exact diagonalization, in the square lattice J_1 - J_2 model, as a function of $\theta = \tan^{-1}(-J_1/J_2)$. The system size is 6×6 .

paper is composed by two ‘decoupled’ Néel-ordered states

$$|\Psi_{\text{CAF}}\rangle = |\Psi_{\text{Neel}}\rangle_{\text{A}} |\Psi_{\text{Neel}}\rangle_{\text{B}}, \quad (56)$$

each of which is defined on a non-frustrated square sublattice coupled with J_2 bonds, say A-sublattice or B-sublattice. For $|\Psi_{\text{Neel}}\rangle$, we employed the variational wavefunction numerically derived by Liang et al.,⁴² which was maximally optimized on the antiferromagnetic square lattice in terms of the staggered magnetic moment, singlet pairing fields, and the Jastrow factor. Note that the expectation value of the ferromagnetic exchange interaction always vanishes in Eq. (56), though the spin-triplet pairing fields connecting the two sublattices could possibly decrease the energy in general. In spite of this, however, the energy of Eq. (56) achieves about 94.5% of the exact ground state energy in 36 spin cluster at $|J_1| = J_2$, whereas it achieves about 96.3% at $J_1 = 0$. We thus regard that, even in the presence of considerable J_1 , Eq. (56) still gives an appropriate energetics for the collinear antiferromagnetic state of the J_1 - J_2 model.

The energy comparison in Fig. 3 shows that the projected Z_2 planar state has the lowest energy in a finite range of the intermediate coupling regime, $0.417|J_1| \lesssim J_2 \lesssim 0.57|J_1|$, whereas the ferromagnetic state is the most stable in the strong J_1 regime, $J_2 \lesssim 0.417|J_1|$, and the collinear antiferromagnetic state is in the strong J_2 regime, $0.57|J_1| \lesssim J_2$. The optimal energy of the planar state projected onto the $S_z = 0$ sector in the 6×6 system achieves roughly 92% \sim 89% of the exact ground state energy obtained by the numerical diagonalization with the same system size. The energy becomes further decreased by 2% \sim 3%, when the wavefunction is projected onto the $S = 0$ space (see Fig. 4).

Figure 3 suggests that, contrary to the mean-field analysis, the projected chiral p -wave state hardly realizes in any of the intermediate coupling regime of the J_1 - J_2 model, at least when the system size is $2n \times 2n$

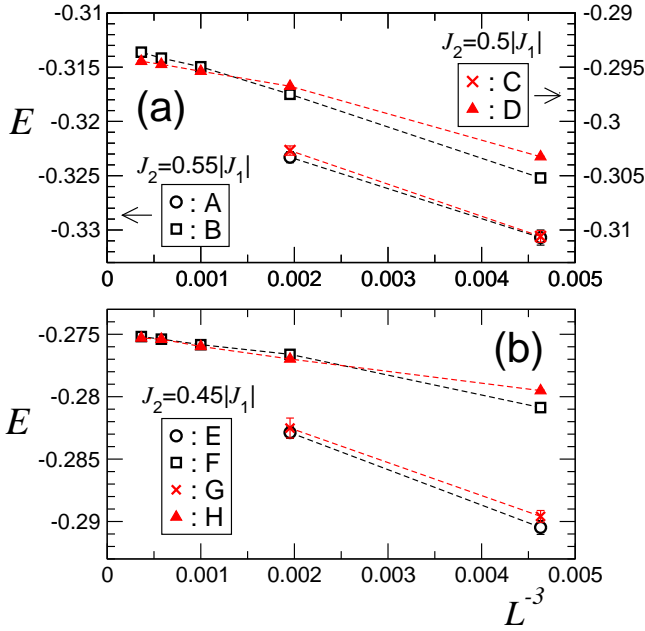


FIG. 5: (Color online) Size dependence of the optimized energies per site for the projected planar states in the $L \times L$ square lattice J_1 - J_2 model with $J_2 = 0.55|J_1|$ (a: black dashed lines), $J_2 = 0.5|J_1|$ (a: red dashed lines), and $J_2 = 0.45|J_1|$ (b). The energy unit is taken to be $\sqrt{J_1^2 + J_2^2}$. The projected states are taken as $\mathcal{P}_{S_z=0}|\Psi_{\text{planar}}\rangle$ ($L = 6 \sim 14$) for the data (B, D, F, H) and as $\mathcal{P}_{S=0}|\Psi_{\text{planar}}\rangle$ ($L = 6, 8$) for the data (A, C, E, G). The horizontal axis is taken as L^{-3} . For $\mathcal{P}_{S_z=0}|\Psi_{\text{planar}}\rangle$ with $L = 14$, we used the same variational parameters as those of $\mathcal{P}_{S_z=0}|\Psi_{\text{planar}}\rangle$ with $L = 12$. For $\mathcal{P}_{S=0}|\Psi_{\text{planar}}\rangle$ with $L = 8$, we used the same variational parameters as those of $\mathcal{P}_{S=0}|\Psi_{\text{planar}}\rangle$ with $L = 6$. The data G and H are calculated in the $(0, \pi)$ -topological sector and the others are in the (π, π) -topological sector.

($n = 3, 4, 5 \dots$). Moreover, the estimated energy of $\mathcal{P}_{S_z=0}|\Psi_{\text{chiral}}\rangle$ is already 30% higher than those of the ferromagnetic state and the projected Z_2 planar state, so that the situation is unlikely reversed, even when the wavefunction is further projected into the singlet space, i.e. $\mathcal{P}_{S=0}|\Psi_{\text{chiral}}\rangle$. Figure 3 also indicates that the Z_2 polar state is almost energetically degenerate with the double π -flux state, which indicates that the spin-triplet pairing does not lower the energy efficiently in this state. Indeed, we observed that the optimized value of the triplet pairing field in the polar state is less than 10% of the root square sum of all the variational parameters.

We also show the system size dependence of the optimized energy per site for the projected planar states in Fig. 5. The data for the state $\mathcal{P}_{S_z=0}|\Psi_{\text{planar}}\rangle$ indicates that the energy has a finite-size correction in the form $E(L)/L^2 = \epsilon_0 - c/L^3$. This observation is consistent with the existence of gapless Goldstone modes in the Z_2 planar state. Using the random phase approximation, we can show that the low energy dispersions of these gapless modes are always linear in the momentum,⁴³ which suggests that the finite-size correction to the ground state

energy per site decays in the form $-c/L^3$, the same as that of the two-dimensional antiferromagnetic Heisenberg model.⁴⁴

V. d -WAVE SPIN-NEMATIC CHARACTER OF PROJECTED Z_2 PLANAR STATES

In this section, we show that all the projected spin-triplet RVB states derived from Eqs. (13,17,21) generally have the ‘spin-nematic’ properties; ordering of quadrupole moments without *spontaneous ordering* of magnetic dipole moments. In particular, we argue that the projected Z_2 planar state has a ‘ d -wave’ spin-nematic character, or an ‘ d -wave’ quadrupolar order, which is consistent with the nature of the spin nematic phase suggested by the exact diagonalization study⁹. All symmetries of the Anderson tower of spin nematic states are clarified from the decomposition of the Z_2 planar state.

To see the ‘spin-nematic’ character, notice first that all the mean-field states discussed in Sec. II are invariant under the spin π -rotation about the 3-axis. Namely, spin-triplet d -vectors in these states are always lying in a plane perpendicular to the field (see Fig. 1), so that the spin π -rotation around the field changes the sign of the triplet pairing fields on the nearest-neighbor ferromagnetic bonds, while leaves intact the singlet pairing fields on the next-nearest-neighbor antiferromagnetic bonds. This sign change can be readily set off by the staggered gauge transformation $f_j^\dagger \rightarrow f_j^\dagger (-1)^{j_x + j_y}$. The whole unitary transformation is expressed as

$$U = \exp \left[i\pi \sum_{j,\sigma} (j_x + j_y) f_{j,\sigma}^\dagger f_{j,\sigma} \right] \times \exp \left[i\frac{\pi}{2} \sum_j f_{j,\alpha}^\dagger [\sigma_3]_{\alpha\beta} f_{j,\beta} \right]. \quad (57)$$

Since the mean-field Hamiltonian is invariant under this transformation, the transformed state $U|g.s.\rangle$ is energetically degenerate with the original ground state $|g.s.\rangle$. On the one hand, being a vacuum state of the Bogoliubov particle, the ground state should be unique, which leads to $U|g.s.\rangle = e^{i\theta}|g.s.\rangle$. Thereby, the projected BCS wavefunction generally satisfies the following relation

$$\langle \{\sigma_j\} | \Psi_\alpha \rangle = \langle \{\sigma_j\} | \mathcal{P} | g.s. \rangle = e^{-i\theta} \langle \{\sigma_j\} | \mathcal{P} U | g.s. \rangle. \quad (58)$$

Since the unitary operator U commutes with the projection \mathcal{P} , the right hand side can be further written as follows with the eigenvalues $S_z \equiv \frac{1}{2} \sum_j \sigma_j$,

$$\langle \{\sigma_j\} | \Psi_\alpha \rangle = e^{-i\theta} e^{i\pi S_z} \langle \{\sigma_j\} | \Psi_\alpha \rangle. \quad (59)$$

One can easily fix the $U(1)$ phase factor, evaluating the product between the projected BCS wavefunctions and a fully polarized state $|\{\sigma_j = 1\}\rangle \equiv \{ \prod_j f_{j,\uparrow}^\dagger \} |0\rangle$,

$$|\langle \{\sigma_j = 1\} | \Psi_\alpha \rangle|^2 = \prod_{\mathbf{k}; k_y > 0} |a_{\mathbf{k}}|^2,$$

where a'_k is defined in Eq. (36). Supposing that a'_k is non-vanishing at any discretized momentum point at $k_y > 0$, which actually holds true for the Z_2 planar state in the zero field case, i.e. Eq. (11), the projected BCS wavefunction has a finite weight in the eigenspace of $S_z = \frac{N}{2}$, $|\langle \{\sigma_j = 1\} | \Psi_\alpha \rangle| \neq 0$. To make this observation compatible with Eq. (59), the phase factor must take a form,

$$e^{-i\theta} = (-1)^{\frac{N}{2}}. \quad (60)$$

In general, we can prove Eqs. (59-60) more directly, only by imposing the spin- π rotational symmetry onto the eigenvectors of a given Bogoliubov Hamiltonian.

Equation (59) guarantees the ‘spin-nematic’ character of the spin-triplet RVB states. Namely, when combined with Eq. (60), this identity requires that the wavefunctions have a finite weight only in the subspace with an even-integer S_z for $N = 4l$ ($l = 1, 2, \dots$) spin systems, whereas only in the subspace with an odd-integer S_z for $N = 4l + 2$ ($l = 0, 1, \dots$) spin systems. Thus, the transverse local magnetization always vanishes in these projected spin-triplet RVB states,

$$\langle \Psi_\alpha | S_{j,\pm} | \Psi_\alpha \rangle = 0, \quad (61)$$

while the spin quadrupole moments in the transverse plane are allowed to have a finite value,

$$\langle \Psi_\alpha | S_{j,+} S_{m,+} | \Psi_\alpha \rangle \equiv f(\mathbf{j} - \mathbf{m}) \neq 0, \quad (62)$$

where $S_{j,+} S_{m,+}$ relates to the spin nematic operators in the form⁹ $S_{j,+} S_{m,+} = (K_{j,m}^{11} - K_{j,m}^{22}) + 2iK_{j,m}^{12}$.

As for the Z_2 planar state derived from Eqs. (11,13), this quadrupole moments obey the d -wave spatial configuration,

$$f(R_{\frac{\pi}{2}}(\mathbf{j} - \mathbf{m})) = -f(\mathbf{j} - \mathbf{m}), \quad (63)$$

where R_θ denotes the space θ -rotation around the axis perpendicular to the square-lattice plane. This d -wave nature comes from the fact that the planar state is invariant under the space $\frac{\pi}{2}$ -rotation accompanied by the spin $\frac{\pi}{2}$ -rotation around the 3-axis (around the field) and the gauge transformation $f_{j,\sigma}^\dagger \rightarrow i(-1)^{j_x+j_y} f_{j,\sigma}^\dagger$. Namely, the state is invariant under the following unitary transformation,

$$U' = \exp \left[i\pi \sum_{j,\sigma} \left(j_x + j_y + \frac{1}{2} \right) f_{j,\sigma}^\dagger f_{j,\sigma} \right] \\ \times \exp \left[i\frac{\pi}{4} \sum_j f_{j,\alpha}^\dagger [\sigma_3]_{\alpha\beta} f_{j,\beta} \right] R_{\frac{\pi}{2}}. \quad (64)$$

Utilizing this symmetry in the same way as we did for the spin π -rotation above, one can derive the following identity for the projected Z_2 planar state,

$$\langle \{\sigma_j\} | \Psi_{\text{planar}} \rangle = (-1)^{\frac{N}{4}} e^{i\frac{\pi}{2} S_z} \langle \{\sigma_{R_{\frac{\pi}{2}}(j)}\} | \Psi_{\text{planar}} \rangle. \quad (65)$$

TABLE I: Indices of the projected Z_2 planar states under the point group symmetries of the square lattice, where N (multiples of 4) denotes the total number of the lattice points.

point group symmetries	$\mathcal{P}_{S_z=2n} \Psi_{\text{planar}} \rangle$
time-reversal (for $n = 0$ and zero-field case)	1
$\frac{\pi}{2}$ -rotation within the lattice	$(-1)^{\frac{N}{4}+n}$
mirror with respect to the x -link	1
translations	1

To obtain the d -wave character from this identity, expand the projected planar state into each S_z -subspace. Under Eq. (59), it takes a form,

$$| \Psi_{\text{planar}} \rangle = \dots + \mathcal{P}_{S_z=-2} | \Psi_{\text{planar}} \rangle + \mathcal{P}_{S_z=0} | \Psi_{\text{planar}} \rangle \\ + \mathcal{P}_{S_z=2} | \Psi_{\text{planar}} \rangle + \mathcal{P}_{S_z=4} | \Psi_{\text{planar}} \rangle + \dots, \quad (66)$$

for $N = 4l$ ($l = 1, 2, \dots$) spins. Among this set of states, the quadrupole operator connects only those two states whose S_z differ by 2,

$$f(\mathbf{j} - \mathbf{m}) = \sum_n \\ \langle \Psi_{\text{planar}} | \mathcal{P}_{S_z=2n+2} S_{j,+} S_{m,+} \mathcal{P}_{S_z=2n} | \Psi_{\text{planar}} \rangle.$$

From Eq. (65), one of these two states is always even under the space $\frac{\pi}{2}$ -rotation, whereas the other is odd. This clearly assigns the d -wave spatial configuration of the quadrupole moments, i.e. Eq. (63).

The arguments so far also suggest how to construct a trial wavefunction for the so-called Anderson’s tower of states (or quasi-degenerate joint states) of the symmetry breaking d -wave spin nematic order under the field. For $N = 4l$ spin clusters, $\mathcal{P}_{S_z=2n} | \Psi_{\text{planar}} \rangle$ mimic the quasi-degenerate joint states (QDJS) of the spin nematic ordered phase, whose representation under the point group symmetry operators are listed in Table. I. These representations are actually consistent with those of the Bose-Einstein condensate phase of a two-magnon bound state near the saturation field.⁹

The projected Z_2 planar state in the zero-field case is time-reversal symmetric; the wavefunction derived from Eq. (11) preserves the following symmetry property,

$$\text{Pf}[\mathbf{X}_{\text{planar}}(\{\sigma_n\})]^* \\ = (-1)^{\frac{N}{2}} \left\{ \prod_j (-1)^{\sigma_j} \right\} \text{Pf}[\mathbf{X}_{\text{planar}}(\{-\sigma_n\})]. \quad (67)$$

To see this relation, notice first that the time-reversal operation changes the sign of the triplet Cooper pairing fields in Eq. (11), while does not affect the singlet pairing fields. Such a sign change can be readily compensated by the previous staggered gauge transformation, $f_j^\dagger \rightarrow f_j^\dagger (-1)^{j_x+j_y}$, which imposes the following relation onto the BCS gap functions:

$$[\mathbf{t}_k]^* = \sigma_2 [\mathbf{t}_{-k+(\pi,\pi)}] \sigma_2.$$

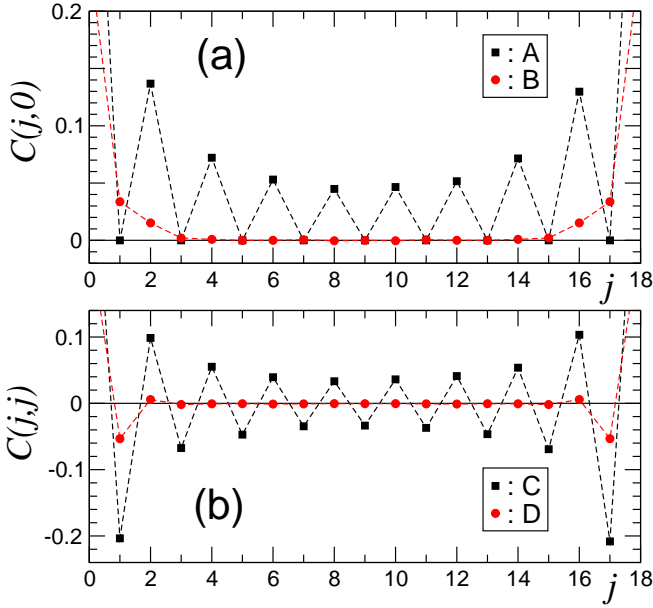


FIG. 6: (Color online) Spin correlation functions of the transverse component $C_{\pm}(j)$ (A and C) and the longitudinal one $C_{zz}(j)$ (B and D) in the projected Z_2 planar state $\mathcal{P}_{S_z=0}|\Psi_{\text{planar}}\rangle$ along (a) the x -direction (1,0) and (b) the diagonal direction (1,1). [A: $C_{\pm}(j,0)$, B: $C_{zz}(j,0)$, C: $C_{\pm}(j,j)$ and D: $C_{zz}(j,j)$.] The projected planar state was obtained in the J_1 - J_2 model with $J_1 = -1$ and $J_2 = 0.45$ in 18×18 spin cluster, which takes the variational parameters as $(D, \chi, \eta) = (0.40, 0.57, 0.72)$. The error-bar is smaller than the symbol.

Or equivalently,

$$\begin{aligned} [\mathbf{X}_{\text{planar}}(\{\sigma_n\})]_{jm}^* &= (-1)^{j_x+j_y} (-1)^{m_x+m_y} \\ &\times (-1)^{\sigma_j} (-1)^{\sigma_m} [\mathbf{X}_{\text{planar}}(\{-\sigma_n\})]_{jm}. \end{aligned}$$

Noting that $\text{Pf}[\mathbf{O}^T \mathbf{A} \mathbf{O}] = \det \mathbf{O} \text{Pf}[\mathbf{A}]$, one immediately obtain Eq. (67). This equation especially means that, as far as $|\Psi_{\text{planar}}\rangle$ is constructed from Eq. (11), both $\mathcal{P}_{S_z=0}|\Psi_{\text{planar}}\rangle$ and $\mathcal{P}_{S=0}|\Psi_{\text{planar}}\rangle$ are even under the time reversal operation for $N = 4l$ spin systems, which is also consistent with the nature of the spin nematic phase suggested by the previous exact diagonalization studies.⁹

VI. STATIC CORRELATION FUNCTIONS

Based on energy comparison and symmetry arguments, we have argued so far that the projected Z_2 planar state is likely to be realized in the square lattice $S = 1/2$ J_1 - J_2 frustrated ferromagnetic model in the intermediate coupling range $0.417|J_1| \lesssim J_2 \lesssim 0.57|J_1|$. To give a direct physical characterization to this intermediate phase, we discuss in this section the static correlation functions calculated with respect to $\mathcal{P}_{S_z=0}|\Psi_{\text{planar}}\rangle$ and $\mathcal{P}_{S=0}|\Psi_{\text{planar}}\rangle$. From the energetics, it is clear that $\mathcal{P}_{S=0}|\Psi_{\text{planar}}\rangle$ is closer to the symmetric ground state of

finite spin clusters than the other in the intermediate phase. On the other hand, the correlation function of $\mathcal{P}_{S_z=0}|\Psi_{\text{planar}}\rangle$ offers a feature of spin-rotational symmetry broken spin nematic state.

Let us begin with the spin correlation function calculated with respect to $\mathcal{P}_{S_z=0}|\Psi_{\text{planar}}\rangle$. In Fig. 6, we show the characteristic behavior of the transverse component of the spin correlation function (labeled as ‘A’ and ‘C’),

$$\begin{aligned} C_{+-}(j-m) &= \frac{1}{2} \langle \Psi_{\text{planar}} | \mathcal{P}_{S_z=0} \{ \hat{S}_{j,+} \hat{S}_{m,-} \\ &\quad + \hat{S}_{j,-} \hat{S}_{m,+} \} \mathcal{P}_{S_z=0} | \Psi_{\text{planar}} \rangle, \end{aligned}$$

and the longitudinal one (labeled as ‘B’ and ‘D’),

$$C_{zz}(j-m) = \langle \Psi_{\text{planar}} | \mathcal{P}_{S_z=0} \hat{S}_{j,z} \hat{S}_{m,z} \mathcal{P}_{S_z=0} | \Psi_{\text{planar}} \rangle.$$

Observing them, notice first that the transverse component of the spin in the A -sublattice in which $j_x + j_y$ is even has no correlation at all with those in the B -sublattice in which $j_x + j_y$ is odd. More generally, this feature holds true for any (projected) Z_2 planar state derived from Eq. (11) or (13), i.e.,

$$\langle \Psi_{\text{planar}} | \{ \hat{S}_{j,+} \hat{S}_{m,-} + \hat{S}_{j,-} \hat{S}_{m,+} \} | \Psi_{\text{planar}} \rangle = 0 \quad (68)$$

for $\forall j \in A$ and $\forall m \in B$. Equation (68) can be understood from the symmetry argument. Suppose that the spin θ -rotation around the z -axis is applied onto all the spins in the A -sublattice, while the spin $-\theta$ -rotation is in the B -sublattice. The mean-field Hamiltonian for the Z_2 planar state is invariant under this continuous transformation, so that the staggered magnetization $S_{A,z} - S_{B,z} = \frac{1}{2} \sum_{j \in A} \sigma_j - \frac{1}{2} \sum_{j \in B} \sigma_j$ is a conserved quantity. Applying this staggered spin rotation to the projected Z_2 planar states, we obtain

$$\langle \{\sigma_j\} | \Psi_{\text{planar}} \rangle = e^{i\theta(S_{A,z} - S_{B,z})} \langle \{\sigma_j\} | \Psi_{\text{planar}} \rangle \quad (69)$$

for any θ . Equivalently, we have

$$\langle \{\sigma_j\} | \Psi_{\text{planar}} \rangle = \delta_{S_{A,z}, S_{B,z}} g(\{\sigma_j\}), \quad (70)$$

which immediately leads to Eq. (68).

Equation (68) suggests that, as for the transverse component of the spin correlation function, the next-nearest-neighbor antiferromagnetic interaction dominates over the competing nearest-neighbor ferromagnetic interaction. In fact, the transverse spin exhibits a strong antiferromagnetic correlation on each of the ‘unfrustrated’ sublattice (square lattice with J_2 bonds), where the function decays nearly in a power-law. (see ‘A’ and ‘C’ in Fig. 6). On the one hand, the longitudinal component always has a ferromagnetic correlation between the nearest neighbor spins and an antiferromagnetic correlation between the 2nd neighbor spins. Thus, the spin-frustration among the ferromagnetic bonds and antiferromagnetic ones effectively suppresses the overall amplitude of the longitudinal correlation function (see ‘B’ and ‘D’ in Fig. 6). Indeed, $C_{zz}(j)$ decays quite rapidly and falls below 10^{-2}

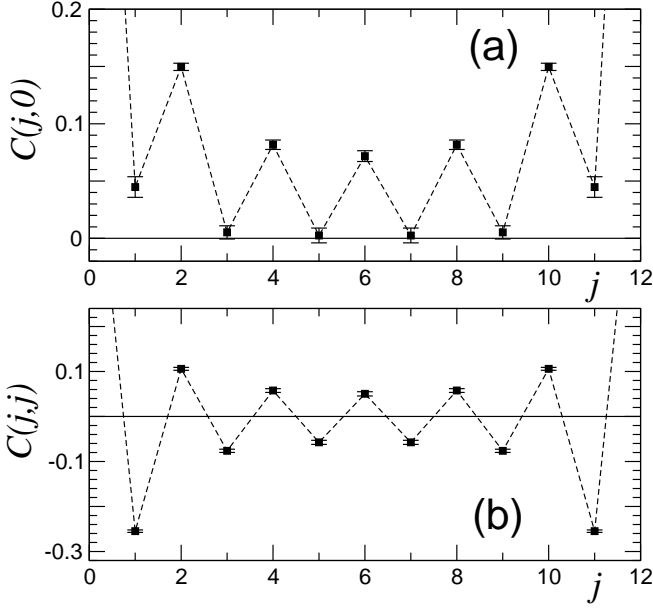


FIG. 7: Spin correlation function $C(j)$ in the spin-singlet state $\mathcal{P}_{S=0}|\Psi_{\text{planar}}\rangle$ along the x -direction (a) and along the diagonal direction (b); [(a) $C(j,0)$ and (b) $C(j,j)$]. The projected planar state was obtained for the J_1 - J_2 model with $J_2 = 0.45|J_1|$ in 12×12 spin cluster, which takes the variational parameters as $(D, \chi, \eta) = (0.45, 0.55, 0.70)$.

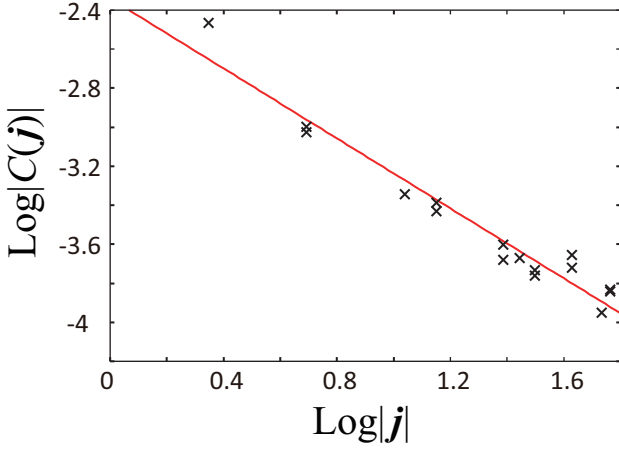


FIG. 8: (Color online) A log-log plot of the correlation function $C(j)$ in the spin-singlet state $\mathcal{P}_{S=0}|\Psi_{\text{planar}}\rangle$ with the same parameter set as used in Fig. 7. We employ only those points with $\max(j_x, j_y) \leq 6$ and $j_x + j_y = \text{even}$. The red solid line indicates the slope of $C(j) \sim (-1)^{j_x} |j|^{-0.9}$.

when the spins are spatially separated by more than two sites, $|j| > 3$.

When the wavefunction is projected onto the spin singlet space, the static spin correlation function

$$C(\mathbf{j} - \mathbf{m}) = \langle \Psi_{\text{planar}} | \mathcal{P}_{S=0} \hat{\mathbf{S}}_{\mathbf{j}} \cdot \hat{\mathbf{S}}_{\mathbf{m}} \mathcal{P}_{S=0} | \Psi_{\text{planar}} \rangle \quad (71)$$

becomes spin-rotational invariant, which ‘interpolate’ between $C_{+-}(j)$ and $C_{zz}(j)$ described above. Namely, as

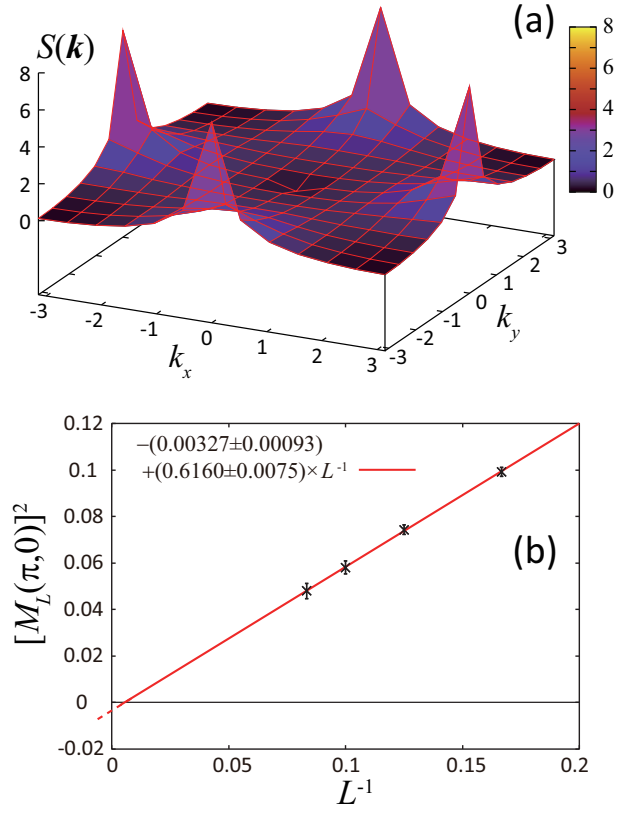


FIG. 9: (Color online) (a) Static spin structure factor $S(\mathbf{k})$ calculated from $\mathcal{P}_{S=0}|\Psi_{\text{planar}}\rangle$ with the same parameter set as used in Fig. 7. The momentum vector \mathbf{k} ranges over the 1st Brillouin zone, $[-\pi, \pi] \times [-\pi, \pi]$. (b) Finite size scaling of $[M_L(\pi, 0)]^2 = \frac{1}{N+2} S(\pi, 0)$ as a function of the linear dimension of the system size, indicating that $M_L(\pi, 0)$ converges to zero in the thermodynamic limit within the statistical error of the Monte Carlo estimation.

shown in Fig. 7, the correlation between the spins in the A -sublattice and those in the B -sublattice are either extremely short-range or almost quenched, while the correlation within each sublattice exhibits an antiferromagnetic ‘quasi-long-ranged’ power law decay, which is fitted as $C(\mathbf{j}) \sim (-1)^{j_x} |\mathbf{j}|^{-\eta}$ with $\eta = 0.9 \sim 1.0$ for $j_x + j_y = \text{even}$ (see Fig. 8). Correspondingly, the static spin structure factor calculated with respect to $\mathcal{P}_{S=0}|\Psi_{\text{planar}}\rangle$

$$S(\mathbf{k}) = \sum_{\mathbf{j}} e^{i\mathbf{k} \cdot \mathbf{j}} C(\mathbf{j}) \quad (72)$$

has characteristic peaks at $(\pi, 0)$ and $(0, \pi)$, while it lose its weight at $(0, 0)$ and (π, π) (see Fig. 9(a)). This behavior resembles the structure factor in the collinear antiferromagnetic phase and seems to be consistent with a recent exact diagonalization study up to 40 sites.²⁰ In spite of the prominent antiferromagnetic fluctuation at $(0, \pi)$ and $(\pi, 0)$, however, the standard finite size scaling fitting of the static spin structure factor^{44,45} suggests that the projected Z_2 planar state does not have any finite

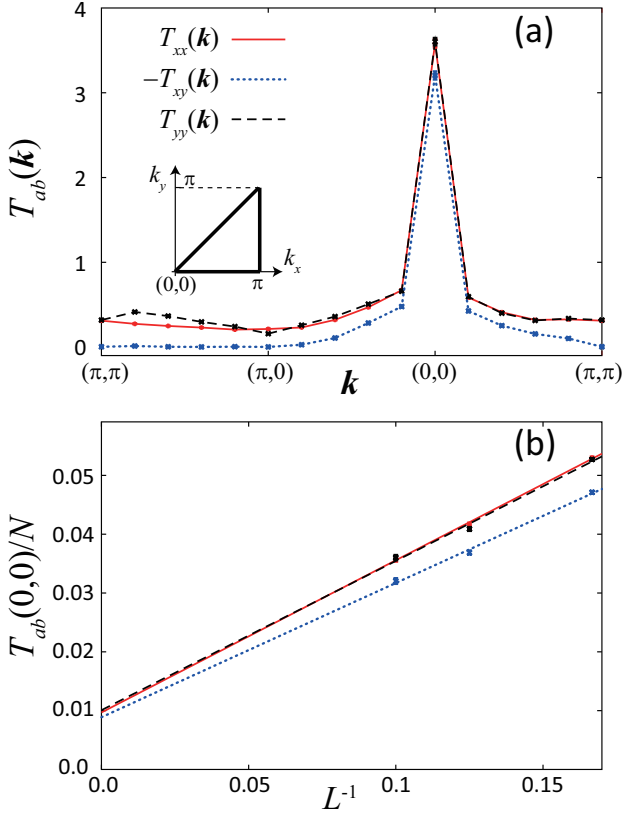


FIG. 10: (Color online) (a) Static structure factor $T_{ab}(\mathbf{k})$ of the quadrupole moments calculated in the projected Z_2 planar state $\mathcal{P}_{S=0}|\Psi_{\text{planar}}\rangle$, with the same parameter set as used in Fig. 7, for the J_1 - J_2 model with $J_2 = 0.45|J_1|$ in 10×10 spin cluster. The (red) solid line depicts the diagonal component $T_{xx}(\mathbf{k})$, the (blue) dotted line the off-diagonal component with minus sign $-T_{xy}(\mathbf{k})$, and the (black) dashed line the other diagonal component $T_{yy}(\mathbf{k})$. Inset: The momentum \mathbf{k} is taken along the high-symmetric momentum points. (b) Finite size scalings of the long-range order of quadrupole moments $\frac{1}{N}T_{ab}(0, 0)$ as a function of $1/L$. The off-diagonal component $T_{xy}(0, 0)$ is shown multiplied by minus sign.

sublattice magnetization $M(\pi, 0)$ in the thermodynamic limit [see Fig. 9(b)];

$$[M(\pi, 0)]^2 = \lim_{L \rightarrow \infty} \frac{1}{L^2 + 2} \sum_j C(\mathbf{j}) e^{i\pi j_x} \simeq 0. \quad (73)$$

The correlation functions of the quadrupole moments are calculated in terms of the projected Z_2 planar state in the spin-singlet subspace,

$$D_{ab}(\mathbf{j} - \mathbf{m}) = \sum_{\mu, \nu=1}^3 \langle \Psi_{\text{planar}} | \mathcal{P}_{S=0} K_{\mathbf{j}, \mathbf{j} + \mathbf{e}_a}^{\mu\nu} \times K_{\mathbf{m}, \mathbf{m} + \mathbf{e}_b}^{\nu\mu} \mathcal{P}_{S=0} | \Psi_{\text{planar}} \rangle \quad (74)$$

with $a, b = x, y$. We found that the diagonal components thus calculated, $D_{xx}(\mathbf{j})$ and $D_{yy}(\mathbf{j})$, are positive-definite for any \mathbf{j} , while the off-diagonal component always takes

a negative value, $D_{xy}(\mathbf{j}) < 0$. In the static structure factor of the quadrupole moments

$$T_{ab}(\mathbf{k}) = \sum_j e^{i\mathbf{k} \cdot \mathbf{j}} D_{ab}(\mathbf{j}), \quad (75)$$

both the diagonal components and (minus of) the off-diagonal component exhibit prominent peaks at the Γ -point [see Fig. 10(a)], indicating the d -wave ordering character of the quadrupole moments in the projected Z_2 planar state. In fact, finite size scalings of their peak values suggest that the state is indeed accompanied by finite quadrupole moments in the thermodynamic limit [see Fig. 10(b)].

VII. SUMMARY AND DISCUSSION

In this paper, we have investigated the phase diagram and the nature of a quantum spin nematic phase in the spin- $\frac{1}{2}$ quantum frustrated J_1 - J_2 model with ferromagnetic J_1 on the square lattice, describing the ground state wavefunction in terms of a spin-triplet pairing state of the spinon fields. Our theory is based on the previous fermionic mean-field analysis,¹⁸ which proposed four types of the mean-field solutions. These solutions include (i) Z_2 planar state, (ii) Z_2 polar state, (iii) $SU(2)$ chiral p -wave state and (iv) ‘flat-band’ state, all of which are characterized by different kinds of spin-triplet pairings of the spinon fields introduced on ferromagnetic bonds. Like in usual ‘projective description’ of symmetric quantum spin liquids,^{1,26,31,32,41} we construct projected BCS wavefunctions out of these triplet pairing states. Performing variational Monte Carlo simulations based on these projected wavefunctions, we obtain the phase diagram Fig. 1 and static correlation functions in the spin nematic wavefunction.

We first argue how these mean-field pairing states are deformed, when external Zeeman field is applied. A direct minimization of the mean-field energy dictates that all the d -vectors in these pairing states are restricted within a plane perpendicular to the applied field. This arrangement makes these pairing states invariant under the spin π -rotation around the magnetic field. Owing to this π -rotational symmetry, the corresponding projected BCS wavefunctions acquire the ‘spin-nematic’ character; ordering of (the transverse component of) the quadrupole moments without any spontaneous ordering of (the transverse) spin moments nor any magnetic crystallization. We also show that the ‘flat-band’ state, which achieves the lowest mean-field energy in the strong ferromagnetic regime $|J_1| \gg J_2$, actually ends up in the trivial fully polarized state, when projected onto the spin Hilbert space.

To examine a possible realization of quantum spin nematic states in the present spin model, we study the energetics of the projected (i) Z_2 planar state, (ii) Z_2 polar state, and (iii) $SU(2)$ chiral p -wave state. We focus especially on the intermediate coupling regime, where the ferromagnetic exchange J_1 is about twice as large as the

antiferromagnetic exchange J_2 , $J_2 \simeq 0.5|J_1|$. Based on the variational Monte Carlo analysis, we argued that, in a finite range of this intermediate coupling regime, the projected Z_2 planar state achieves the best optimized energy, compared with the energies of other competing phases, such as the ferromagnetic phase and collinear antiferromagnetic phase. (See Fig. 1.) We also prove that this projected Z_2 planar state is accompanied by the ‘ d -wave’ spatial configuration of the quadrupole moments. This feature of the wavefunction including the irreducible representations under the symmetry group turns out to show a perfect agreement with the nature of the quantum spin nematic phase suggested by Shannon *et al.*⁹ from the exact diagonalization study.

Motivated by this coincidence, we further calculate the spin-spin correlation function of the projected Z_2 planar state, so as to obtain the static spin structure factor in the spin nematic phase. The structure factor thus calculated exhibits two prominent peaks at the wavevectors $\mathbf{k} = (\pi, 0)$ and $(0, \pi)$, which signifies the presence of strong collinear antiferromagnetic fluctuation. The finite size scaling of the peak height concludes that the state does not possess any sublattice magnetization in the thermodynamic limit, which is consistent with the spin-nematic feature of the Z_2 planar state. This antiferromagnetic fluctuation is reminiscent of the neighboring collinear antiferromagnetic phase, whereas ferromagnetic fluctuation, which is also expected to appear from the other neighboring ferromagnetic phase, is completely suppressed.

These observations indicate that the static spin-spin correlation function by itself hardly distinguishes the

current quantum spin nematic phase from the neighboring collinear antiferromagnetic phase. Indeed, the recent exact diagonalization study by Richter *et al.*²⁰ reported that the present J_1 – J_2 model exhibits only a strong collinear antiferromagnetic correlation in the intermediate coupling regime, $J_2 \simeq 0.5|J_1|$. We expect that the dynamical magnetic properties in combination with these static physical properties could distinguish the present spin nematic phase from the collinear antiferromagnetic phase. That is, unlike in the collinear antiferromagnetic phase, all the gapless Goldstone modes in the spin-nematic phase are expected to lose their spectral weight in the dynamical spin structure factor in the low-energy limit. In fact, a recent calculation based on the random phase approximation shows that this is indeed the case in the Z_2 planar state.⁴³ This feature could be sharply contrasted to the dynamical magnetic property in the collinear antiferromagnetic phase, where the gapless mode at the $(0, \pi)$ -point or $(\pi, 0)$ -point have a finite spectral weight even in the low-energy limit.

Acknowledgments

We acknowledge Masatoshi Imada, Yukitoshi Motome, Takashi Koretsune, Philippe Sindzingre, and Leon Balents for helpful discussions. RS was partially supported by the Institute of Physical and Chemical Research (RIKEN). This work was supported by Grants-in-Aid for Scientific Research from MEXT, Japan (No. 22014016 and No. 23540397).

-
- ¹ X. G. Wen, *Quantum Field Theory of Many-Body Systems*, (Oxford University Press, Oxford, 2004).
- ² P. Fazekas and P. W. Anderson, *Philosophical Magazine* **30**, 423-440 (1974); P. W. Anderson, *Science* **235**, 1196 (1987).
- ³ L. Balents, *Nature* **464**, 199 (2010); P. A. Lee, *Science* **321**, 1306, (2008).
- ⁴ G. Misguich and C. Lhuillier, in *Frustrated Spin Systems*, edited by H. T. Diep (World Scientific, Singapore, 2004).
- ⁵ K. Ishida, M. Morishita, K. Yawata, and Hiroshi Fukuyama, *Phys. Rev. Lett.* **79**, 3451 (1997).
- ⁶ R. Masutomi, Y. Karaki, and H. Ishimoto, *Phys. Rev. Lett.* **92**, 025301 (2004).
- ⁷ M. Roger, J. M. Delrieu, and J. H. Hetherington, *Phys. Rev. Lett.* **45**, 137 (1980); *Rev. Mod. Phys.* **55**, 1 (1983).
- ⁸ A. F. Andreev and I. A. Grishchuk, *Sov. Phys. JETP* **60**, 267 (1984).
- ⁹ N. Shannon, T. Momoi, and P. Sindzingre, *Phys. Rev. Lett.* **96**, 027213 (2006); P. Sindzingre, N. Shannon, and T. Momoi, *J. Magn. Magn. Mater.* **310**, 1340 (2007).
- ¹⁰ P. Sindzingre, L. Seabra, N. Shannon, and T. Momoi, *J. Phys. Conf. Ser.* **145**, 012048 (2009).
- ¹¹ P. Sindzingre, N. Shannon, and T. Momoi, *J. Phys. Conf. Ser.* **200**, 022058 (2010).
- ¹² T. Momoi and N. Shannon, *Prog. Theor. Phys. Suppl.* **159**, 72 (2005).
- ¹³ T. Momoi, P. Sindzingre, and N. Shannon, *Phys. Rev. Lett.* **97**, 257204 (2006).
- ¹⁴ D. V. Dmitriev, V. Ya. Krivnov, and A. A. Ovchinnikov, *Phys. Rev. B* **55**, 3620 (1997).
- ¹⁵ N. Shannon, B. Schmidt, K. Penc, and P. Thalmeier, *Eur. Phys. J. B* **38**, 599 (2004).
- ¹⁶ B. Schmidt, N. Shannon, and P. Thalmeier, *J. Phys.: Condens. Matter* **19**, 145211 (2007); *J. Magn. Magn. Mater.* **310**, 1231 (2007).
- ¹⁷ J. R. Viana and J. R. de Souza, *Phys. Rev. B* **75**, 052403 (2007).
- ¹⁸ R. Shindou and T. Momoi, *Phys. Rev. B* **80**, 064410 (2009).
- ¹⁹ M. Härtel, J. Richter, D. Ihle, and S.-L. Drechsler *Phys. Rev. B* **81**, 174421 (2010).
- ²⁰ J. Richter, R. Darradi, J. Schulenburg, D. J. J. Farnell, and H. Rosner, *Phys. Rev. B* **81**, 177429 (2010).
- ²¹ P. Chandra, P. Coleman, and A. I. Larkin, *Phys. Rev. Lett.* **64**, 88 (1990).
- ²² A. V. Chubukov, *Phys. Rev. B* **44**, 4693 (1991).
- ²³ P. Chandra and P. Coleman, *Phys. Rev. Lett.* **66**, 100 (1991); P. Chandra, P. Coleman, and A. I. Larkin, *J. Phys. Condens. Matter* **2**, 7933 (1990).
- ²⁴ E. Fradkin, *Field Theories of Condensed Matter Systems*

- (Addison-Wesley, London, 1991).
- ²⁵ Assa Auerbach, *Interacting electrons and Quantum Magnetism* (Springer-Verlag, New York, 1994).
- ²⁶ G. Baskaran, Z. Zou, P. W. Anderson, Solid State Communication **63**, 973 (1987); G. Baskaran and P. W. Anderson Phys. Rev. B **37**, 580 (1988); E. Dagotto, E. Fradkin, and A. Moreo, Phys. Rev. B **38**, 2926 (1988).
- ²⁷ Quantum spin states with spin-triplet pairing of fermions are explored also in $S \geq 1$ quantum spin systems; Zheng-Xin Liu, Yi Zhou, and Tai-Kai Ng, Phys. Rev. B **82**, 144422 (2010).
- ²⁸ In Ref. 18, we called the planar state as the (two-dimensional analogue of) Balian-Werthamer state and the polar state as the collinear state. In this paper, we adopt ‘planar/polar’ instead, since they seem to be more familiar in the standard literature such as Refs. 29 and 30.
- ²⁹ D. Vollhardt and P. Wolfe, *The Superfluids Phase of Helium 3*, (Taylor & Francis, 1990).
- ³⁰ G. E. Volovik, *The universe in a Helium droplet*, (Oxford University Press, 2003).
- ³¹ J. B. Marston and I. Affleck, Phys. Rev. B **39**, 11538 (1989); I. Affleck and J. B. Marston, Phys. Rev. B **37**, 3774 (1988).
- ³² C. Gros, Annals of Physics **189**, 53 (1989); B. Edegger, V. N. Muthukumar, and C. Gros, Advances in Physics, **56**, 927 (2007).
- ³³ S. Sorella, Phys. Rev. B **64**, 024512 (2001); M. Casula and S. Sorella, J. Chem. Phys. **119**, 6500 (2003); M. Casula, C. Attaccalite, and S. Sorella, J. Chem. Phys. **121**, 7110 (2004); S. Yunoki and S. Sorella, Phys. Rev. B **74**, 014408 (2006).
- ³⁴ Claudia Filippi and Stephen Fahy, J. Chem. Phys. **112**, 3523 (2000); C. J. Umrigar and Claudia Filippi, Phys. Rev. Lett. **94**, 150201 (2005).
- ³⁵ J. P. Bouchaud, A. Georges, and C. Lhuillier, J. Phys. (Paris) **49**, 553 (1988)
- ³⁶ M. Bajdich, L. Mitas, L. K. Wagner, and K. E. Schmidt, Phys. Rev. B **77**, 115112 (2008).
- ³⁷ See for example Fig. 3 in Ref. 9.
- ³⁸ D. Tahara and M. Imada, J. Phys. Soc. Jpn. **77**, 114701 (2008).
- ³⁹ P. Ring and P. Schuck, *The Nuclear Many-Body Problem* (Springer, Heidelberg, 1980); T. Mizusaki and M. Imada, Phys. Rev. B **69**, 125110 (2004); F. F. Assaad, P. Werner, P. Corboz, E. Gull, and M. Troyer, Phys. Rev. B **72**, 224518 (2005); T. Aimi and M. Imada, J. Phys. Soc. Jpn. **76**, 084709 (2007).
- ⁴⁰ M. Abramowitz and I. A. Stegun, *Handbook of Mathematical Functions*, Applied Mathematics Series, Vol. **55**, 916 (Washington: National Bureau of Standards; reprinted 1968 by Dover Publications, New York).
- ⁴¹ C. Gros, Phys. Rev. B **38**, 931 (1988); F. C. Zhang, C. Gros, T. M. Rice, and H. Shiba, Supercond. Sci. Technol. **1**, 36 (1988).
- ⁴² S. Liang, B. Doucot, and P. W. Anderson, Phys. Rev. Lett, **61**, 365 (1988).
- ⁴³ R. Shindou, S. Yunoki, and T. Momoi, arXiv:XXXX
- ⁴⁴ D. Huse, Phys. Rev. B **37**, 2380 (R) (1988).
- ⁴⁵ H. J. Schulz and T. A. L. Ziman, Europhysics Letter **18**, 355 (1992); H. J. Schulz, T. A. L. Ziman, and D. Poilblanc, J. Phys. I **6**, 675 (1996); J. Richter and J. Schulenburg, Eur. Phys. J. B **73**, 117 (2010).